

# Late-time critical behavior of local string-like observables under quantum quenches

Souvik Bandyopadhyay<sup>1,\*</sup>, Anatoli Polkovnikov<sup>2</sup>, and Amit Dutta<sup>1</sup>

<sup>1</sup>*Department of Physics, Indian Institute of Technology Kanpur, Kanpur 208016, India and*

<sup>2</sup>*Department of Physics, Boston University, Boston, Massachusetts 02215, USA*

In recent times it has been observed that signatures of equilibrium quantum criticality surprisingly show up in many-body systems which are manifestly far from equilibrium. We explore such scenarios in interacting spin systems subject to a quench and develop a robust method to systematically probe ground state critical physics through nonequilibrium post-quench dynamics. Analyzing late-time behavior of finite string-like observables, we find emerging sharp signatures of equilibrium criticality. Specifically, these observables accurately detect equilibrium critical points and universal critical exponents after long times following a quench. This happens despite the fact that the analyzed systems are chaotic/ergodic and is interestingly due to a strong memory of the initial conditions retained by these observables after quench. We find that our results can also be used to explain critical signatures in post-quench domain formation, seen in a recent experiment with trapped ion quantum simulators.

## I. INTRODUCTION

Understanding phase transitions have been a central theme in the study of many body statistical mechanics. A plethora of studies into the nature and classification of phase transitions [1–3] has led to a comprehensive theoretical and experimental understanding of the phenomena. Phase transitions are known to manifest as nonanalyticities in free energy densities at finite temperatures and energy at very low temperatures. Furthermore, it has been well established that a critical system exhibits a diverging correlation length in the thermodynamic limit and obeys universal scaling laws which are not dependent on microscopic details of the system. Similar to thermal phase transitions driven by thermal fluctuations, a class of phase transitions in the zero temperature ground state of quantum many-body systems have also been discovered [4, 5]. These quantum phase transitions (QPTs) are solely driven by quantum fluctuations arising from competing mechanisms, resulting in different favored ground states in different phases. Interestingly, QPTs are also accompanied by a diverging correlation length near criticality and follow universal scaling laws (see Ref. [6] for a review). Apart from equilibrium quantum phase transitions, recent studies have led to the discovery of a new type of quantum criticality exclusive to out of equilibrium systems [7]. Known as dynamical quantum phase transitions [8–15], these extend the concept of criticality and universality to the early time dynamics of nonequilibrium systems, which are far from their ground states.

Even so, it is usually difficult to understand how equilibrium critical phenomena can manifest in generic high energy excited states of a system. In this light, there has been an extensive search for footprints of quantum criticality in excited and particularly out of

equilibrium systems [16–31]. Particularly, Ref. [24, 25] and very recently Ref. [26, 30], report signatures of equilibrium criticality following a quench, which manifest in late time observables and higher order correlations. It is remarkable that some of these signatures of quantum phase transitions persist even after chaotic scrambling in quenched systems. On the other hand, a recent quenching experiment in a trapped ion quantum simulator, has also detected signatures of equilibrium QPTs; these are manifested in the late time domain statistics of a quenched chaotic system of interacting spins [17]. Nonetheless, a generic theoretical origin of these surprising signatures of equilibrium criticality in systems manifestly far from equilibrium has remained elusive as yet.

In this work, we set out to develop a unified theory connecting several recent experimental and theoretical observations on such nonequilibrium signatures of quantum criticality, particularly those reported in Refs. [17, 26]. We note that the theory also naturally explains the recently observed critical behavior of local probes, such as magnetization density, following chaotic quenches (see Ref. [24, 32]). We begin by demonstrating that the time averaged Loschmidt echo (LE), a nonequilibrium analogue of the partition function, develops sharp signatures following a sudden quench when the quenched Hamiltonian crosses an equilibrium critical point in both integrable (also seen in Refs. [33, 34]) and chaotic systems. Additionally, we observe that the time averaged LE satisfies universal finite size scaling laws as the quenched Hamiltonian approaches the critical point following a generic quantum quench. To understand the definition of the LE, consider a system in a many body initial state  $|\psi(0)\rangle$  allowed to evolve unitarily with a quenched Hamiltonian  $H$ ; the Loschmidt echo following the sudden quench is then defined as,  $\mathcal{L} = |\langle\psi(0)|\psi(t)\rangle|^2 = |\langle\psi(0)|\exp[-iHt]|\psi(0)\rangle|^2$ . However, as evident from its definition, due to an exponentially growing basis with system size, the LE is very difficult to probe experimentally in many body

---

\* souvik@iitk.ac.in

systems.

We therefore proceed to systematically construct experimentally accessible and time-insensitive local probes, out of string type observables, which capture critical behavior in quenched quantum systems. We find that mimicking the behavior of the LE, sharp signatures indicative of the equilibrium critical point can also emerge as a function of the quenching parameter in time averaged string observables. Recently, such operators have been shown to efficiently detect dynamical critical behavior and early time singularities in both integrable and chaotic out of equilibrium systems [14, 35, 36]. By construction, these local string operators eventually approach the projector onto the complete initial state as their spatial support (string length) increases. Following a quantum quench, the string observables are expected to reach a steady state after sufficiently long times. Specifically, for integrable quenches, generic local observables are known to eventually relax into a generalized Gibbs ensemble in a thermodynamically large system [37, 38]. On the other hand, if  $H$  is chaotic, the system eventually thermalizes and expectation values of local observables can be described by a microcanonical ensemble. This is in accordance with the eigenstate thermalization hypothesis (ETH) [39–42]. Thus, expectation values of generic local observables are expected to be smooth functions of energy, containing no information of the initial state [43] except energy density. In contrast to the long time behavior of LE, it is therefore unlikely for local observables to develop true nonanalyticities in their bare expectations following chaotic quenches. Nevertheless, we find that, even after a sufficiently long ergodic evolution, the observables remarkably hold strong and stable memory of the initial state. Besides, the string observables are also found to have much longer life-times in chaotic eigenstates in comparison to single-site observables such as magnetization density. Consequently, after sufficiently long times following the quench, we see robust and sharp signatures of the equilibrium QCP in the local probes, even with bilinear observables, as found numerically in Ref. [26]. We therefore show that string observables indeed allow us to systematically access zero temperature ground state properties, such as phase transitions in quenching experiments [17], without having to actually prepare the system in its ground state.

Interestingly, we further observe that the long time averaged string observables also satisfy critical scaling relations with the string length following near critical quenches even in chaotic systems. This allows us to directly determine critical exponents associated with the equilibrium QCPs in the long time behavior of the local observables. Moreover, we find that the simple time averaged expectation of the string operators reveal a much deeper connection with the probability of domain formation in the post quench system. To elaborate, the time averaged projectors are nothing but the probability

distribution of domains in the asymptotic state, thus enabling us to perform a complete statistical analysis of polarized and unpolarized domain formation, in the post-quench system. This connection in turn, assigns a direct experimental meaning to the string observables and at the same time shed light on the origin of these sharp critical signatures in quenching experiments. We find that not only does the domain statistics reveal the position of equilibrium QCPs accurately, they also theoretically explain the recent experimental findings [17] on a quantum simulator [44].

To further probe the sensitivity of the results on the choice of the initial state of the system, we analyze the long time averaged infinite temperature correlators of the string observables. Particularly, we show that the time averaged infinite temperature auto correlation and out of time ordered correlators (OTOC) also detect the equilibrium QCP sharply. This establishes that the sharp signatures in string observables detecting equilibrium QCPs, are in general insensitive to any specific choice of initial states in quenching experiments. In recent times, infinite temperature OTOCs of local observables have also become instrumental in the study of information scrambling [45–47] and dynamical phases [36] in chaotic many body systems. Furthermore, OTOCs have been experimentally measured in ultracold atomic lattices through various echo protocols [48–52]. As we demonstrate our ideas through the experimentally accessible quantum Ising model of spins [53], our claims are readily verifiable in state of the art quantum simulators.

The paper is organized in the following sections: In Sec. II we introduce the model system and elaborate on the quenching protocol employed in the rest of the paper to demonstrate the results. Section. III contains a study of the complete analytic structure of the time averaged Loschmidt echo when the system is quenched to a QCP in the integrable limit. In Sec. IV, we define the local string operators and demonstrate critical behavior of their long time average following both integrable and chaotic quenches. In Sec. V, we proceed to show that the time averaged LE along with the local string observables follow appropriate scaling laws near the equilibrium QCPs and calculate universal critical exponents characterizing the QCPs. In Sec. VI, we probe the late time statistics of finite strings and show how it connects with recent experimental data on ultracold ion lattices measuring domain statistics following a quench in interacting spin systems. Sec. VII describes the infinite temperature two-time correlators of the string operators as they develop sharp signatures at equilibrium QCPs, following both integrable and chaotic quenches. In Sec. VIII we elaborate on the origin of the strong initial state memory in string observables following ergodic evolution. Finally, we conclude in Sec. IX with a brief summary of the important results and possible future directions of investigation.

## II. MODEL SYSTEM AND QUENCHING PROTOCOL

To demonstrate the efficacy of string operators and the LE in capturing quantum critical physics in quenched systems, we use a ferromagnetic axial next nearest neighbor (ANNNI) model [5], with nearest neighbor interactions and next nearest neighbor interactions, both ferromagnetic, and a transverse external field  $h$ . Such a system having  $L$  spins can be described completely by the many-body Hamiltonian,

$$H = - \sum_{i=1}^L \sigma_i^x \sigma_{i+1}^x - J_2 \sum_{i=1}^L \sigma_i^x \sigma_{i+2}^x - h \sum_{i=1}^L \sigma_i^z, \quad (1)$$

where  $J_2 > 0$  and  $\sigma_i$  represent Pauli matrices at the  $i^{\text{th}}$  site. For numerical advantage, we have used periodic boundary conditions, such that  $\sigma_{L+i} \equiv \sigma_i$ . The line  $J_2 = 0$  in the parameter space is the well known integrable transverse field Ising model with quantum critical points (QCPs)  $h = \pm 1$ , separating paramagnetic and ferromagnetic phases in a thermodynamically large ( $L \rightarrow \infty$ ) system. Interestingly, the system still hosts an Ising critical line separating the ferromagnetic phase from a paramagnetic phase in the plane of parameters  $J_2$  and  $h$ . Under this choice of the parameters, the Ising critical line is given by a transcendental equation in  $J_2$  and  $h$  (see Refs. [9, 54]),

$$1 + 2J_2 = h + \frac{J_2 h^2}{2(1 + J_2)}. \quad (2)$$

As one approaches the integrable point  $J_2 \rightarrow 0$ , the critical point drifts towards the critical point of the transverse Ising model, i.e.,  $h = 1$ . The Ising phase transition is known to reflect a spontaneous breaking of a global  $Z_2$  symmetry due to spin inversion, in the ordered (ferromagnetic) phase ground state. This allows the longitudinal magnetization density in the ground state to serve as an appropriate order parameter, which is nonzero in the ordered phase while vanishes in the paramagnetic phase.

We analyze quench dynamics starting from an initial state  $|\psi(0)\rangle$  and inflict a sudden quench in the transverse field at a time  $t = 0$ , thereby allowing the system to evolve with the final quenched Hamiltonian. Following such a quench, the long time expectation value of local observables  $O$  in the thermodynamic limit approaches the average given by the diagonal ensemble (see Ref. [41]),

$$\lim_{t \rightarrow \infty} \langle \psi(t) | O | \psi(t) \rangle = \sum_{\alpha} |\langle \psi(0) | \phi_{\alpha} \rangle|^2 \langle \phi_{\alpha} | O | \phi_{\alpha} \rangle, \quad (3)$$

where the states  $|\phi_{\alpha}\rangle$  are the eigenstates of the quenched Hamiltonian  $H$ . For nonintegrable quenches, because the system is ergodic, the expectation values of local observables  $\langle \phi_{\alpha} | O | \phi_{\alpha} \rangle$  are essentially given by corresponding microcanonical averages. By the central limit theorem, the probabilities to occupy different energy states

$|\langle \psi(0) | \phi_{\alpha} \rangle|^2$  are expected to be peaked around mean energy, i.e. near  $E_{\alpha} = \bar{E} \equiv \langle \psi_0 | H | \psi_0 \rangle$ . From this argument, any memory of the initial state except for the total mean energy of the system and perhaps its variance, determining the width of the energy distribution, should be lost. However, we will show that for string observables these simple considerations are not completely valid. Even though in accordance with ETH, the mean state to state fluctuations of these observables in nearby eigenstates decrease with system size, we see a very rapid rise in their relative variance within a narrow energy shell with increasing string size. These increasing fluctuations prevent a purely thermal description of comparatively longer strings and encode a persistent memory of the initial state even after chaotic quenches. Because of these large fluctuations, we further show that long string observables take comparatively longer to relax and have highly oscillating late-time connected auto-correlation functions in chaotic eigenstates.

## III. TIME AVERAGED LOSCHMIDT ECHO FOLLOWING AN INTEGRABLE QUENCH

In this section, we discuss the complete analytic structure of the time averaged Loschmidt echo following a quench at the integrable point. We start from the ground state of  $H_0 \equiv H(J_2 = 0, h_i)$  and quench the system at time  $t = 0$  to a final set of parameters  $H \equiv H(J_2 = 0, h)$ . Allowing the system to evolve with the quenched Hamiltonian, we then probe the long time averaged LE,

$$\bar{\mathcal{L}} = \lim_{T \rightarrow \infty} \frac{1}{T} \int_0^T dt |\langle \psi(0) | \psi(t) \rangle|^2. \quad (4)$$

Expanding in terms of the eigenstates of the Hamiltonian  $H |\phi_{\alpha}\rangle = E_{\alpha} |\phi_{\alpha}\rangle$  and carrying out the integration one therefore arrives at,

$$\mathcal{O}_L \equiv -\frac{1}{L} \log \bar{\mathcal{L}} = -\frac{1}{L} \log \sum_{\alpha} |\langle \psi(0) | \phi_{\alpha} \rangle|^4. \quad (5)$$

In Fig. 1 we plot  $\mathcal{O}_L$  as a function of  $h$  and observe that it becomes nonanalytic at the equilibrium critical points, where its first derivative with respect to  $h$  develops a discontinuous jump. In Appendix. A we show that in the thermodynamic limit Eq. (5) can be represented through the following contour integral of the complex variable  $z = e^{zk}$  over the circle  $C \equiv |z| = 1$ :

$$\mathcal{O}_L = \frac{1}{2\pi i} \oint_C F(h, z) dz, \quad (6)$$

where

$$F(h, z) = \frac{1}{z} \log \left[ 1 - \frac{h^2 (z^2 - 1)^2}{8z(h+z)(hz+1)} \right]. \quad (7)$$

To understand the origin of the nonanalyticity of  $\mathcal{O}_L$  it is easier to analyze its derivative with respect to  $h$ :

$$\partial_h \mathcal{O}_L = \frac{1}{2\pi i} \oint_C \partial_h F dz. \quad (8)$$

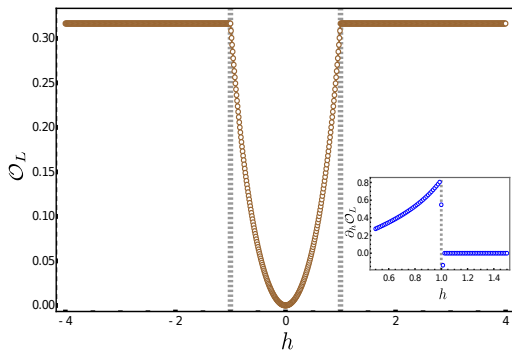


Figure 1. The rate function of the time averaged Loschmidt echo  $\mathcal{O}_L$  develops nonanalyticities at equilibrium QCPs, in the thermodynamic limit as a function of the quenched (final) transverse field starting from the ground state of the integrable Hamiltonian  $H_0$ .

As evident from Eq. (7), the function  $\partial_h F$  has simple poles on the real axis at  $z_1 = -1/h$  and  $z_2 = -h$ , which cross at the QCP  $h = h_c = 1$ , as well as some additional poles, which are not sensitive to  $h_c$ . In Fig. 2 we show the movement of these poles in the complex plane with the quenched field  $h$ , near the critical point corresponding to the singularity at  $h_c = 1$  and  $z = -1$ . The residues corresponding to these poles are  $\text{Res}(z = z_1) = -1/h$  and  $\text{Res}(z = z_2) = 1/h$  (see Appendix. A for details). As  $h$  crosses  $h_c$  the poles entering the integration contour switch causing the integral to jump leading to the cusp singularity in  $\mathcal{O}_L(h)$  shown in Fig. 1.

#### IV. TIME AVERAGED EXPECTATION OF LOCAL PROJECTORS

As discussed in Sec. I, it is in general difficult to experimentally probe the LE in macroscopic systems. We therefore proceed to define local scalable string operators  $P_n$  of finite length  $n$  defined such that as  $n$  increases their expectation values  $\mathcal{L}_n$  approach the Loschmidt echo. Specifically we define

$$\mathcal{L}_n(t) = \langle \psi(t) | P_n | \psi(t) \rangle, \quad (9)$$

where,

$$P_n = \frac{1}{L} \sum_{i=1}^L \frac{1}{2^n} \prod_i^{i+n} (\mathbb{I}_i + \sigma_i^x). \quad (10)$$

Clearly for  $n = L$  we recover the complete Loschmidt echo for the fully polarized initial state corresponding to  $h_i = 0$ ,

$$\mathcal{L}_L(t) = \langle \psi(t) | P_L | \psi(t) \rangle = |\langle \psi(0) | \psi(t) \rangle|^2. \quad (11)$$

Note that one can add to  $P_n$  a similar operator projecting to the down spin state composed of products of  $(\mathbb{I}_i - \sigma_i^x)$ .

Following an integrable quench ( $J_2 = 0$ ) at  $t = 0$  starting from the ground state at  $h_i = 0$  to  $h$ , we next analyze the long time averages of the projectors  $\mathcal{L}_n$ :

$$\mathcal{O}_n = -\frac{1}{n} \log \overline{\mathcal{L}_n(t)}, \quad \overline{\mathcal{L}_n(t)} = \lim_{T \rightarrow \infty} \frac{1}{T} \int_0^T dt \mathcal{L}_n(t). \quad (12)$$

According to Eq. (3) the function  $\overline{\mathcal{L}_n(t)}$  can be expressed as a weighted expectation value of the string operator  $P_n$  in the eigenstates of the quenched Hamiltonian  $H$ . In Fig. 3(a) we observe sharp nonanalyticities developing in  $\mathcal{O}_2$ ,  $\mathcal{O}_3$  and  $\mathcal{O}_4$  in the thermodynamic limit, which we also compare to exact diagonalization results in finite systems obtained using the QuSpin package [55, 56]. Further, Fig. 3(a) also compares the infinite and finite time averages of the observables  $\mathcal{L}_n(t)$  showing robustness of the observed nonanalyticities to the duration of the time-averaging window. Fig. 3(b) shows the jump discontinuities following critical quenches in the first derivative response  $\partial_h \mathcal{O}_n$  for finite strings (see Appendix. B for a detailed analytical derivation). For numerical advantage, in Fig. 3(a)-3(b), the initial state has been chosen to be the even parity ground state at  $h_i = 0$ . Although the operator  $P_L$  projects onto the completely polarized state  $|\rightarrow \rightarrow \rightarrow \dots\rangle$ , which is not a parity eigenstate, the transitions detecting equilibrium QCPs are still manifested in the observables.

It is also evident that the sharp signatures detecting the QCP in the string observables are not exclusive to integrable systems. To demonstrate this, we numerically analyze quenches to a nonintegrable Hamiltonian ( $J_2 = 0.1$ ) starting from the same polarized initial state. In Fig. 4, we show the results for  $\mathcal{O}_n$  when averaged over sufficiently long times and the full time averaged Loschmidt echo corresponding to  $n = L$ . Both the LE and the observable  $\mathcal{O}_n$  develops a sharp singularity at the transition point  $h = h_c \approx 1.14$  for the chosen parameters. We note that despite a relatively small integrability breaking coupling used in the simulation we are able to accurately detect the corresponding small shift of the position of the QCP given by Eq. (2) despite high energy dumped into the system during the quench.

#### V. UNIVERSAL SCALING LAWS FOLLOWING CRITICAL QUENCHES

Given the sharp behavior of string observables detecting equilibrium criticality, it is natural to ask whether the time-insensitive local probes also capture universal physics near equilibrium QCPs following a quench. Starting with the long time averaged Loschmidt echo, we address this question by studying how the string observables behave under scaling transformations near critical quenches. Specifically, close to the equilibrium critical

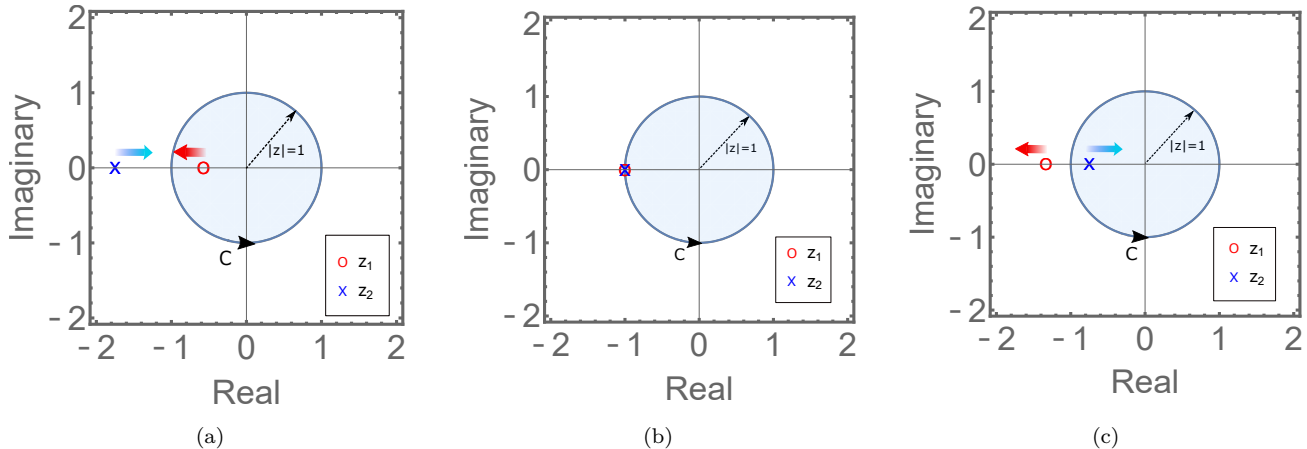


Figure 2. The positions of the poles  $z_1$  and  $z_2$  of the function  $\partial_h F(h, z)$  (see Eq. (7)), which elucidate the analytic structure of the Loschmidt echo  $\mathcal{O}_L$ . The arrows indicate the drift of the poles as one approaches the ferromagnetic phase from the paramagnetic phase, i.e., as  $h$  decreases. The three panels correspond to an integrable quench to (a)  $h = 1.5$  (paramagnetic), (b)  $h = 1$  (critical) and (c)  $h = 0.75$  (ferromagnetic), starting from the ferromagnetic ground state at  $h_i = 0$ . The unimodular circle  $C$  represents the contour of integration employed in evaluating the derivative in Eq. (6).

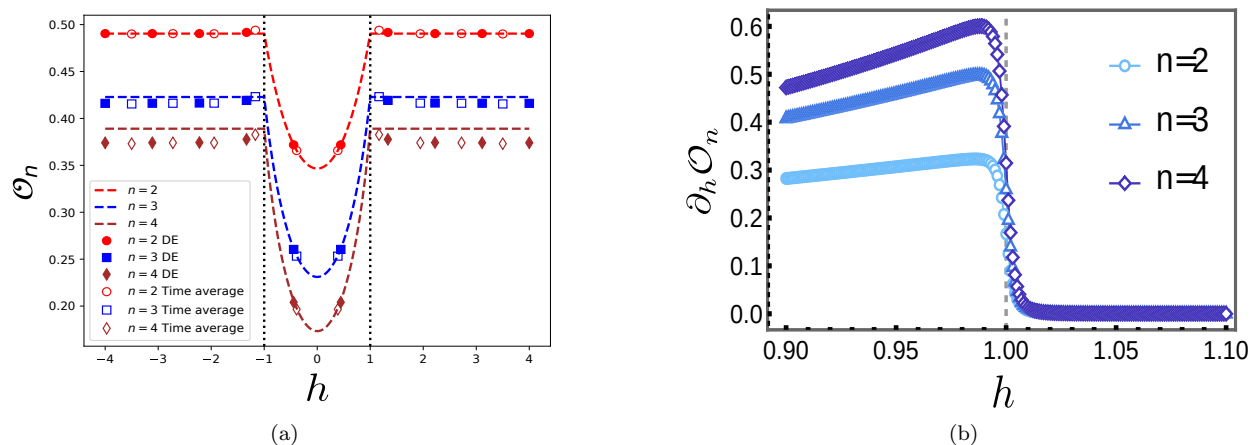


Figure 3. (a) The observables  $\mathcal{O}_n$  develop nonanalyticities at quantum critical points, following a quench of the transverse field in an integrable model in the thermodynamic limit (shown in dashed lines). The discrete points show the corresponding quantities in a system with  $L = 16$  spins, calculated using exact diagonalization. The solid (hollow) symbols represent the diagonal ensemble averaged (time averaged) quantities. To simplify calculations, only the even spin parity sector has been considered and all time averaging has been performed up to  $T = 30$  starting from the ground state at  $h_i = 0$ . (b) Jump singularities at the critical point  $h = 1.0$  in the first derivative of the local observables  $\mathcal{O}_n$ , following an integrable quench in the thermodynamic limit. Exact analytical calculations of the discontinuous jumps have been presented in Appendix. B.

point  $h = h_c + \delta$ , we estimate the singular part of the observable  $\mathcal{O}_L$  by a universal function under scaling transformations  $\delta \rightarrow L^{1/\nu}\delta$ . Namely, in the finite size scaling regime ( $L^{1/\nu}|\delta| \ll 1$ ), the singular part of the time averaged LE is observed to scale as,

$$\mathcal{O}_L(L^{-1}, \delta) \sim L^{-\alpha/\nu} \Phi(L^{1/\nu}\delta), \quad (13)$$

where  $\nu$  and  $\alpha$  are critical exponents and  $\Phi$  is an universal scaling function (see Appendix. C for a detailed discussion on the scaling form). In Fig. 4(b) and Fig. 5(a) we show a finite size scaling collapse following a nonintegrable and

integrable quench, respectively. In the finite-size scaling regime, the transition in  $\mathcal{O}_L$  for different system sizes is seen to collapse near the equilibrium critical point into a single function for the scaling exponents  $\nu = \alpha = 1$ , thus verifying the scaling relation in Eq. (13). We therefore find that the sharpness of the transition detected by  $\mathcal{O}_L$  exhibit a universal approach to a true nonanalyticity as one approaches the thermodynamic limit.

Also, due to the emergence of a nonanalyticity at equilibrium QCPs, the second derivative  $|\partial_h^2 \mathcal{O}_L|$  diverges in

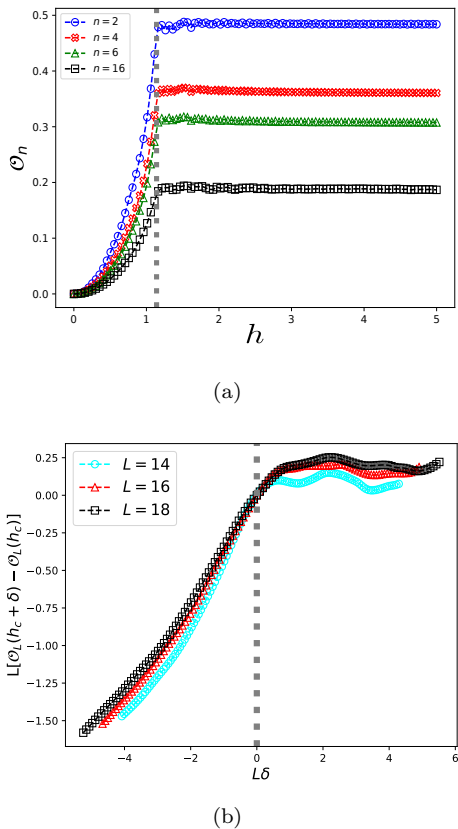


Figure 4. (a) The observables  $\mathcal{O}_n$  for finite projectors of length  $n$  in the nonintegrable ANNNI model ( $J_2 = 0.1$ ) exhibit sharp transitions at the Ising QCP ( $h \approx 1.1$ ) in a system of  $L = 16$  spins. (b) Finite size scaling collapse of  $\mathcal{O}_L$  near the critical point (see Eq. (13)) for the nonintegrable quench. All the time averages have been performed up to  $T = 30$  following the quench from a completely polarized initial state.

the thermodynamic limit. In the finite size scaling regime, owing to the scaling form in Eq. (13), we expect the second derivative near the QCP to diverge as,

$$|\partial_\delta^2 \mathcal{O}_L| \sim L^{\frac{2-\alpha}{\nu}} \Psi(\delta^{1/\nu} L), \quad (14)$$

in the regime  $L^{1/\nu} \delta \ll 1$ , for some dimensionless scaling function  $\Psi$ . Therefore, for an Ising critical point, the quantity  $|\partial_\delta^2 \mathcal{O}_L|$  diverges polynomially in the thermodynamic limit as,

$$|\partial_\delta^2 \mathcal{O}_L| \sim L \Psi(\delta L), \quad (15)$$

near the critical point. This scaling behavior has been verified in Fig. 5(b), where the rescaled derivative response  $L^{-1} \partial_\delta^2 \mathcal{O}_L$  when plotted against  $\delta L$  shows a good collapse near the critical point for different system sizes.

Moving on to the finite projectors  $P_n$  ( $n < L$ ), due to the introduction of another length scale  $n$ , we assume a modified scaling ansatz (see also Appendix. B we analytically probe the scaling form following integrable quenches)

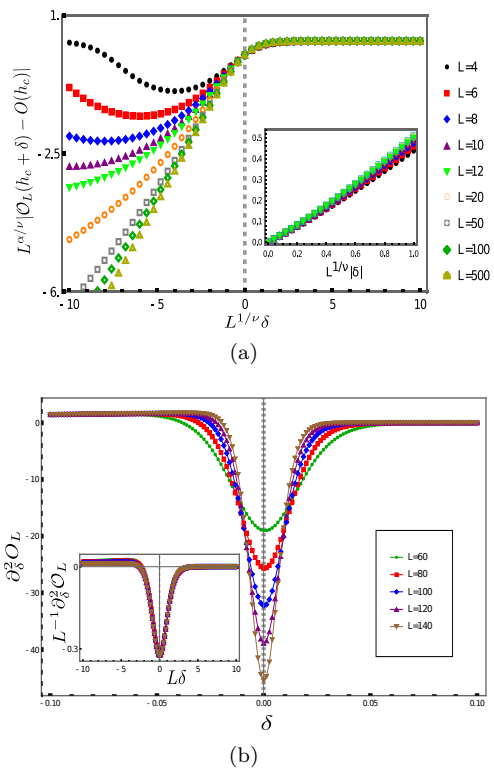


Figure 5. (a) Finite size scaling of the observable  $\mathcal{O}_L$  when the averaging is done over the diagonal ensemble, following an integrable quench starting from the ground state at  $h_i = 0$ . On choosing the critical exponents to be  $\nu = \alpha = 1$  (see Eq. (13)), all data points for different  $L$  collapse into a single scaling function near the critical point. (Inset) Zoomed-in image of the finite-size scaling collapse near the critical point ( $L^{1/\nu} \delta \ll 1$ ) for the same critical exponents. (b) The second derivative of  $\mathcal{O}_L$  diverges with increasing system size near the QCP. (Inset) Scaling collapse of the rescaled derivative response  $L^{-1} \partial_\delta^2 \mathcal{O}_L$  near the critical point (see Eq.(15)).

near an equilibrium QCP in the limit  $n \ll L$ ,

$$\mathcal{O}_n = n^{-\alpha/\nu} \Pi(n^{1/\nu} \delta), \quad (16)$$

where  $\Pi$  is a dimensionless scaling function. Similar to the finite size scaling of the full projectors  $\mathcal{O}_L$ , in Fig. 6(a)-6(b) we show that the data for  $\mathcal{O}_n$  having different string sizes  $n$ , collapse under scaling transformations with the exponents  $\alpha = \nu = 1$  for both integrable and chaotic quenches. This allows us to extract universal critical information following a quench using the string observables in a scalable approach. Furthermore this suggests that by measuring string expectations accessible to measurements which are local in space and time, it is possible to accurately determine the universality class of equilibrium QCPs in generic quenching experiments.

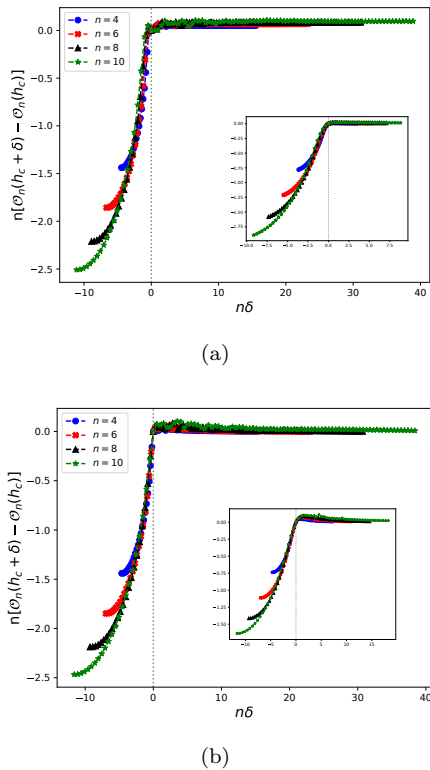


Figure 6. (a) The finite string observables  $\mathcal{O}_n$  collapse near the equilibrium QCP in the integrable regime ( $J_2 = 0$ ) following a quench from a completely polarized ferromagnetic ground state at  $h = 0$ . The time averaging has been done over the interval  $[0, T = 30]$  in a chain of  $L = 16$  spins. (Inset) Scaling collapse of  $\mathcal{O}_n$  near the QCP when averaged over the diagonal ensemble, i.e., for  $T \rightarrow \infty$ . (b) The scaling collapse of  $\mathcal{O}_n$  near the Ising critical point in the nonintegrable regime ( $J_2 = 0.1$ ) averaged over the same time window as in (a). (Inset) The corresponding DE average shows a similar collapse under scaling transformations.

## VI. STATISTICS OF FINITE STRINGS

To further assign an experimental relevance to the string observables, we look for post quench signatures of the critical point in the statistics of local strings with a close connection to recent experimental results. Particularly, using site resolved fluorescence imaging of trapped-ion lattices, Ref. [17] shows that it is indeed possible to directly measure domain formation probabilities in a post-quench many-body spin system. We numerically simulate such quenching experiments and probe the connection of the proposed string operators with domain formation probabilities.

In generic many-body spin systems product states  $|\mathcal{F}_i\rangle = \bigotimes_j |s_j^i\rangle$  such that  $s_j^i = \rightarrow$  or  $\leftarrow$ , span the complete Hilbert space  $\mathcal{H}$  of the system. It is then easily seen that the finite projectors  $P_n$ ,  $n \leq L$ , acting on a generic state  $|\psi\rangle$ , projects it to the subspace  $\mathcal{A}_n \subseteq \mathcal{H}$  of

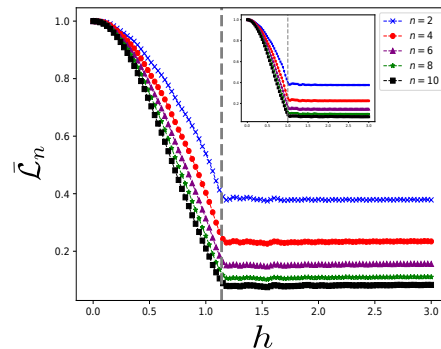


Figure 7. The time averaged probability distribution  $\bar{\mathcal{L}}_n$  to find  $\rightarrow$ -polarized strings of length  $n$  or greater in the post quench state as a function of the quenched transverse field  $h$ .  $\bar{\mathcal{L}}_n$  shows a sharp transition as the quenched field  $h$  crosses the equilibrium QCP in the nonintegrable setting ( $J_2 = 0.1$ ). (Inset) The distribution  $\bar{\mathcal{L}}_n$  against the quenched field following a quench in the integrable Ising limit ( $J_2 = 0$ ). The time averaging has been performed up to  $T = 30$  in a chain of  $L = 16$  spins and the exact critical point has been represented by vertical dashed lines.

all product states containing  $\rightarrow$ -polarized spin clusters of length  $l^+ \geq n$ . That is, for a generic many-body state

$$|\psi\rangle = \sum_i c_i |\mathcal{F}_i\rangle, \quad (17)$$

where  $c_i = \langle \mathcal{F}_i | \psi \rangle$ , the expectation of the finite projectors can be written as

$$\langle \psi | P_n | \psi \rangle = \sum_{i: |\mathcal{F}_i\rangle \in \mathcal{H}} |c_i|^2 p_i = \sum_{i: |\mathcal{F}_i\rangle \in \mathcal{A}_n} |c_i|^2, \quad (18)$$

where  $p_i$  is either 0 or 1 corresponding to whether the state  $|\mathcal{F}_i\rangle$  contains the polarized string of length  $l^+ \geq n$  or not. The expectation  $\langle \psi | P_n | \psi \rangle$  therefore is nothing but the probability to find the  $\rightarrow$ -polarized strings of length  $l^+ \geq n$  in the state  $|\psi\rangle$ . Therefore, in a quenching experiment the expectation  $\mathcal{L}_n(t)$  of the projectors in the time evolved state  $|\psi(t)\rangle$  (see Eq. (9)) essentially capture real time domain formation probabilities in the post-quench system. Consequently the infinite time averaged distributions  $\bar{\mathcal{L}}_n$  (as defined in Eq. (12)) following a quench, describe the probability of detecting polarized domains in the diagonal ensemble.

While obtaining numerical results using exact diagonalization, we average over finite but sufficiently long times. In Fig. 7, we observe the finitely long time averaged distribution  $\bar{\mathcal{L}}_n$  following a quench starting from the completely polarized initial state  $|\rightarrow\rightarrow\dots\rangle$  in both integrable and chaotic systems. We note that unlike ferromagnetic quenches, the distribution varies very slowly with the quenched field as one enters the paramagnetic phase. This shows a sharp contrast between quenches to the ordered and the disordered

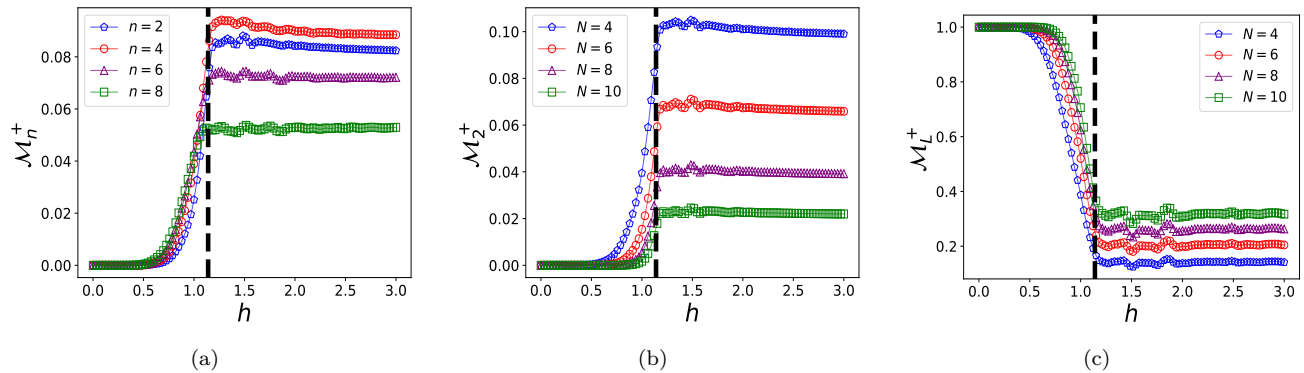


Figure 8. (a) The probability  $\mathcal{M}_n^+$  (see Eq. (21)) that the longest string observed after  $N = 10$  uncorrelated measurements has a length  $n$  in the post quench state, as a function of the quenched transverse field  $h$ . The noise in the data for quenches into the disordered phase is an artifact of finite system size (see Appendix. D for a detailed discussion). (b) The transition in  $\mathcal{M}_n^+$  becomes sharper as one increases the number of measurements  $N$ , shown for a single string of length  $n = 2$ . (c) The distribution of full length domains  $\mathcal{M}_L^+$  with respect to the quenched field also shows a sharp change as the quenched field crosses the equilibrium QCP in the nonintegrable situation. In all the simulations the time averaging has been performed up to  $T = 30$  starting from a completely  $\rightarrow$ -polarized initial state in the chaotic ANNNI model ( $J_2 = 0.1$ ) of  $L = 18$  spins. In all the panels, the exact critical point has been shown by a vertical dashed line.

phase. Even with comparatively smaller strings we see sharp signatures accurately detecting the equilibrium critical point in the post quench distribution of polarized spin clusters.

*Statistics of polarized spin clusters:* Owing the physical meaning of  $\bar{\mathcal{L}}_n$  it is convenient to introduce the following notation:

$$\bar{\mathcal{L}}_n = \rho(l^+ \geq n), \quad (19)$$

with  $\rho(l^+ \geq n)$  representing the probability of finding  $\rightarrow -$ strings of length  $l^+ = n$  or greater in the late time post quench state of the system. This implies that  $1 - \bar{\mathcal{L}}_n = 1 - \rho(l^+ \geq n) = \rho(l^+ < n)$  is the probability of finding polarized strings of length  $n - 1$  or smaller, after sufficiently long times following a quench. Therefore

$$\rho(l^+ \leq n) = 1 - \bar{\mathcal{L}}_{n+1}. \quad (20)$$

Now consider  $N$  independent measurements on the system determining the late time spin configurations following a sudden quench, as is generically employed in experiments with ultracold atomic lattices [17]. In this setting, we proceed to find the probability that the longest  $\rightarrow -$ polarized string observed after all the independent measurements has a length  $n$  as,

$$\begin{aligned} \mathcal{M}_n^+(N) &= \rho(l^+ \leq n)^N - \rho(l^+ \leq n-1)^N \\ &= (1 - \bar{\mathcal{L}}_{n+1})^N - (1 - \bar{\mathcal{L}}_n)^N. \end{aligned} \quad (21)$$

In Fig. 8(a), we observe that for quenches in the ferromagnetic phase, the distribution  $\mathcal{M}_n^+(N = 10)$  is very close to zero for finite  $n$ , while it shows a sharp transition into a slowly varying distribution as the

quenched field drifts into the disordered phase. Also, as seen in Fig. 8(b), this sharp transition detecting the equilibrium QCPs becomes sharper as one increases the number of measurements  $N$ . From this behavior of the string distributions, we infer that for quenches into the ordered phase, it is most likely that the longest  $\rightarrow -$ string observed in the late-time state has the maximum length  $L$  (see Fig. 8(c)).

Further, using Eq. (20), it is also possible to theoretically calculate exclusive probabilities  $\mathcal{Q}_n^+$  that a  $\rightarrow$ -polarized string of length exactly equal to  $n$  is contained in a late-time single-shot measurement in quenching experiments,

$$\begin{aligned} \mathcal{Q}_n^+ &= \rho(l^+ = n) = \bar{\mathcal{L}}_n - \bar{\mathcal{L}}_{n+1}, \quad n = 0, 1, \dots, L-1, \\ \mathcal{Q}_L^+ &= \rho(l^+ = L) = \bar{\mathcal{L}}_L. \end{aligned} \quad (22)$$

such that,

$$\bar{\mathcal{L}}_n = 1 - \sum_{s=0}^{n-1} \mathcal{Q}_s^+. \quad (23)$$

We now proceed to demonstrate the behavior of the mean maximum domain length of  $\rightarrow$ -polarized spins in the late-time state following  $N$  independent measurements:

$$\overline{n_{max}} = \sum_{s=0}^L s \mathcal{M}_s^+(N). \quad (24)$$

Fig. 9(a) shows that, for quenches into the ordered phase, the mean longest  $\rightarrow$ -string is very close to the system size  $L$ . Near the quench to the critical point  $\overline{n_{max}}$  rapidly drops to a minimum and then starts growing again as we further increase the quench amplitude, but very slowly.

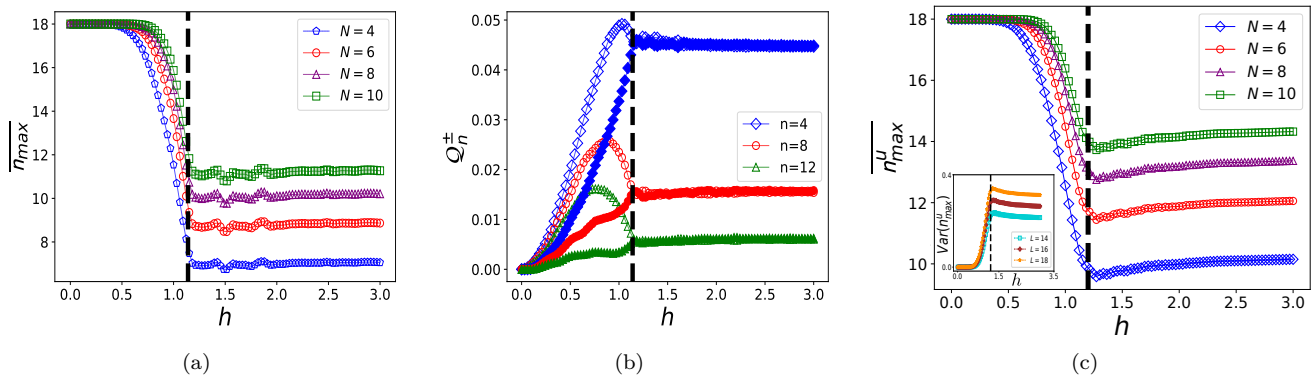


Figure 9. (a) The mean longest  $\rightarrow$ -polarized string  $\overline{n_{max}}$  observed after  $N$  independent measurements shows a sharp transition as the quenched field  $h$  crosses the equilibrium quantum critical point in a chaotic system of  $L = 18$  spins. (b) For quenches into the paramagnetic phase both  $\rightarrow$  and  $\leftarrow$ -polarized strings contribute equally after long times. The hollow (solid) symbols representing the single shot measurement probabilities  $Q_n^+$  ( $Q_n^-$ ) collapse for a particular string length  $n$  when the quenched field lies in the disordered phase. The time averaging has been done up to  $T = 30$  following a quench starting from the completely polarized state  $|\rightarrow\rightarrow\dots\rangle$  for  $L = 16$  spins. (c) The mean longest size of unpolarized domains after  $N$  measurements show a prominent dip precisely near the critical point in a system of size  $L = 18$ . (Inset) The coefficient of variation of the maximum domain length after  $N = 10$  uncorrelated measurements showing a maxima for a critical quench in the nonintegrable setup for different system sizes,  $L = 14, 16$  and  $18$ .

(see a more detailed discussion in Appendix E.)

*Statistics of unpolarized spin clusters:* Similar to the distributions  $\tilde{L}_n$  of  $\rightarrow$ -polarized domains, we now construct the time averaged distribution of  $\leftarrow$ -polarized strings following a quench as  $\tilde{L}_n^-$ . The probabilities  $\tilde{L}_n^-$  are simply given by time averaged expectation of the strings,

$$P_n^- = \frac{1}{L} \sum_{i=1}^L \frac{1}{2^n} \prod_i^{i+n} (\mathbb{I}_i - \sigma_i^z). \quad (25)$$

projecting onto  $\leftarrow$ -polarized clusters of length  $l^- \geq n$ . Following Eq. (22), one can now proceed to define exclusive probability distributions  $Q_n^-$  of detecting a  $\leftarrow$ -string having length  $l^- \geq n$  in the post quench state such that,

$$\sum_{s=0}^L Q_s^- = 1. \quad (26)$$

In Fig. 9(b) we observe that in contrast to quenches into the ordered phase, for quenches into the paramagnetic phase both  $\rightarrow$  and  $\leftarrow$ -strings of finite lengths become equally probable in the late-time state of the system. This behavior can be understood physically by noting that at small amplitude quenches starting from a completely polarized ground state  $|\rightarrow\rightarrow\dots\rangle$  only large domains of the same polarization are likely to appear. Interestingly the probabilities of creating left- and right-domains meet exactly at the transition point and remain essentially identical after that. We note that this behavior of domain distributions is also consistent with a recent study in quenched chaotic systems [24], reporting the vanishing of time averaged local magnetization, following

quenches into the disordered phase (see Appendix F). Furthermore, it is apparent from Fig. 9(b) that even after a long time chaotic evolution, the distributions  $Q_n^\pm$  show a clear bias towards the polarized initial state for quenches into the ordered phase.

Equipped with the independent distributions of detecting polarized  $\rightarrow$  /  $\leftarrow$ -domains, we next proceed to construct joint distributions of detecting a  $\rightarrow$ -polarized string having length  $l^+ = n$  and a  $\leftarrow$ -polarized string having length  $l^- = m$  simultaneously in a single measurement,

$$Q(n, m) = \rho(l^+ = n \cap l^- = m) = Q_n^+ Q_m^-. \quad (27)$$

Using Eq. (23) and Eq. (26), it can then be easily verified that the joint probabilities also satisfy the completeness criteria,

$$\sum_{n, m=0}^L Q(n, m) = 1. \quad (28)$$

This in turn allows us to explicitly write down probability distributions that the longest unpolarized string observed after  $N$  independent measurements has a length  $n$  as,

$$\begin{aligned} \mathcal{M}_n(N) &= \left( \sum_{r, s=0}^n Q(r, s) \right)^N - \left( \sum_{r, s=0}^{n-1} Q(r, s) \right)^N, \\ \mathcal{M}_L(N) &= 1 - [(1 - Q_L^+) (1 - Q_L^-)]^N. \end{aligned} \quad (29)$$

Similar to the mean longest  $\rightarrow$ -polarized string length, we now find the mean longest unpolarized domain length observed after  $N$  independent measurements in the post

quench state as,

$$\overline{n_{\max}^u} = \sum_{s=0}^L s \mathcal{M}_s(N). \quad (30)$$

In Fig. 9(c), we show that the mean longest domain size exhibits a minima precisely at the equilibrium QCP which allows a good experimental determination of the critical point in quenching experiments. We note that the dip in the mean longest domain length at the equilibrium critical point persists with increasing system size. Moreover, the minima of the mean maximum domain length near a critical quench, was recently observed in Ref. [17] using a quantum simulator. The string observables therefore offer a comprehensive understanding of the recent experimental findings. At the same time, the coefficient of variation/relative deviation of the maximum domain length,

$$\text{Var}(n_{\max}^u) = \frac{\sigma(n_{\max}^u)}{n_{\max}^u}, \quad (31)$$

$\sigma$  denoting the standard deviation of the longest domain length in the late-time state, also shows a maxima when the system is quenched to the critical point. Recently, the domain statistics of polarized spins have also been seen [35, 36, 57] to detect dynamical quantum phase transitions in the early time behavior of an Ising system. It can thus be inferred that the statistics of string observables provide strong and generic markers of quantum criticality in out-of-equilibrium states and at the same time are directly accessible to present day experimental setups.

## VII. INFINITE TEMPERATURE UNEQUAL TIME CORRELATIONS

Apart from the equal time expectations, we now proceed to examine the various two-time probes constructed out of string operators which are manifestly insensitive to the choice of the initial state in quenching setups. The infinite temperature auto-correlation and OTOC of the string operators provide a good testbed for this purpose, as they are experimentally measurable in optical lattices and at the same time contain no information of the initial state of the system. Particularly, we consider the long time averages of the infinite temperature auto-correlation and OTOCs,

$$\begin{aligned} \mathcal{D}_n &= -\frac{1}{n} \log \lim_{T \rightarrow \infty} \frac{1}{T} \int_0^T dt \text{Tr} [P_n(t) P_n(0)], \\ \mathcal{C}_n &= -\frac{1}{n} \log \lim_{T \rightarrow \infty} \frac{1}{T} \int_0^T dt \text{Tr} [P_n(t) P_n(0) P_n(t)]. \end{aligned} \quad (32)$$

Note that for extensive projectors, i.e., when the string sizes span the complete chain, we recover the full

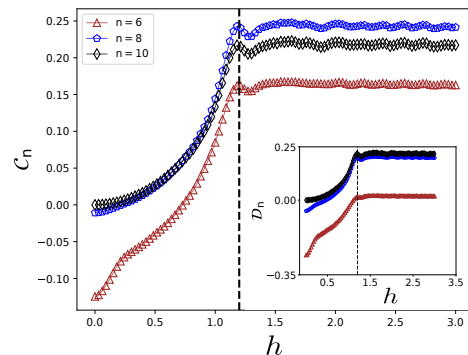


Figure 10. Logarithmic infinite temperature time averaged OTOC following a quench to a transverse field  $h$  starting from a completely polarized state  $|\rightarrow \rightarrow \dots\rangle$  in the nonintegrable ANNNI model. The OTOC is seen to develop a sharp transition at the equilibrium critical point  $h_c \approx 1.14$  for  $J_2 = 0.1$ . (Inset) Sharp signatures in the corresponding logarithmic auto correlation function. In both the simulations, the time averaging has been done up to  $T = 20$  in a chain of  $L = 10$  spins.

Loschmidt echo from these infinite temperature probes,

$$\begin{aligned} \text{Tr} [P_L(t) P_L(0)] &= \langle \psi_0 | P_L(t) | \psi_0 \rangle = \mathcal{L}_L(t), \\ \text{Tr} [P_L(t) P_L(0) P_L(t)] &= \text{Tr} [P_L(0) P_L(-t) P_L(0)] \\ &= \langle \psi_0 | P_L(-t) | \psi_0 \rangle = \mathcal{L}_L(-t). \end{aligned} \quad (33)$$

Also, for the local strings ( $n < L$ ), the time averages in Eq. (32) can be replaced by averages over all eigenstates  $|\phi_\alpha\rangle$  of the quenched Hamiltonian, such that

$$\frac{e^{-n\mathcal{D}_n}}{2^L} = \overline{\langle \phi_\alpha | P_n | \phi_\alpha \rangle^2}, \quad (34)$$

represents the second moment of the distribution of diagonal matrix elements  $\langle \phi_\alpha | P_n | \phi_\alpha \rangle$  over the spectrum of the quenched Hamiltonian  $H$ . Eq. (34) further reflects the fact, that the averaged correlators are completely insensitive to both initial state information and time. Similarly, the long time averaged OTOC in Eq. (32) reduces to a time-insensitive weighted average over all eigenstates  $|\phi_\alpha\rangle$ ,

$$\frac{e^{-n\mathcal{C}_n}}{2^L} = \overline{\langle \phi_\alpha | P_n | \phi_\alpha \rangle \langle \phi_\alpha | P_n^2 | \phi_\alpha \rangle} \quad (35)$$

In Fig. 10, we see that similar to  $\mathcal{O}_n$ , finitely long time averaged correlations  $\mathcal{C}_n$  and  $\mathcal{D}_n$  develop sharp signatures near the equilibrium critical point following a nonintegrable quench. We therefore conclude that the late time behavior of the OTOC following a quench, approaches the nonanalyticity of the full Loschmidt echo at equilibrium QCPs with increasing string size. Thus detecting the QCP sharply in both integrable and chaotic quenched systems. This suggests that the critical behavior of the string operators is indeed generic and depend only on the final quenched Hamiltonian,

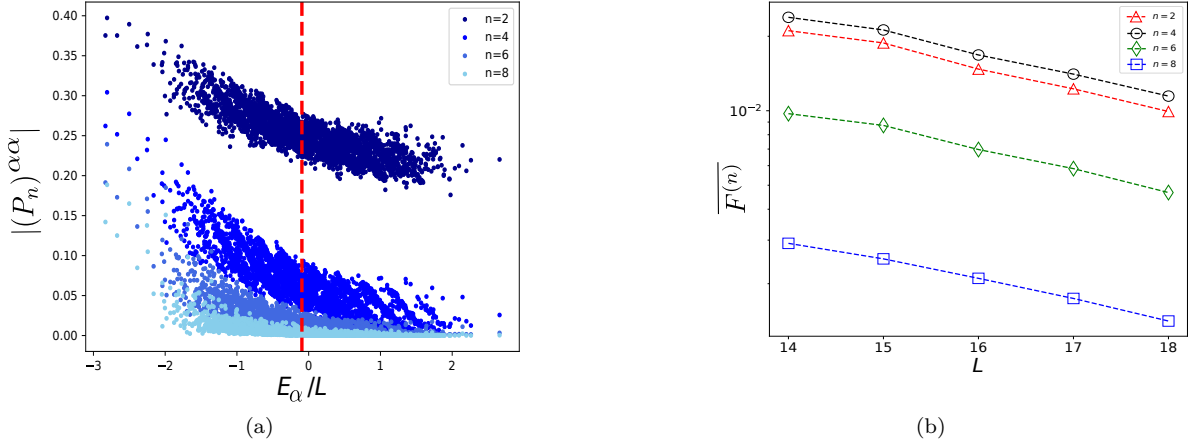


Figure 11. (a) The distribution of diagonal matrix elements of the local projectors  $P_n$  when plotted against energy density in the eigenspace of a quenched chaotic ANNNI Hamiltonian, shows a diminishing contribution of excited states with increasing string lengths. Starting from an initial ground state of the Hamiltonian (see Eq. (1)) for  $J_2 = 1.0$ ,  $h = 2$ , the system is quenched to  $J_2 = 1.0$ ,  $h = -2.5$  in a chain of  $L = 16$  spins. These quench parameters have been chosen such that the mean energy after the quench (marked by the vertical dashed line) lies near the middle of the spectrum, where we have a sufficiently high density of states. (b) Mean state-to-state fluctuation of the operators  $P_n$  in nearby eigenstates, averaged over 50% of the eigenstates centered about the mean energy after quench.

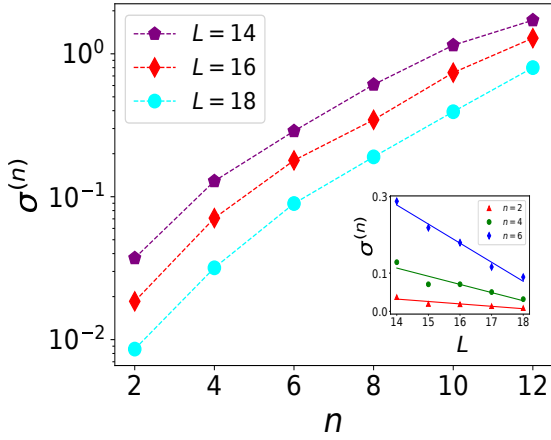


Figure 12. Relative fluctuation of the diagonal matrix elements of string observables against string length  $n$ , within a small energy shell of half-width  $\delta E = 0.1\sqrt{L}$  about the mean energy  $\bar{E}$ . (Inset) The relative fluctuations decay with system size very slowly with increasing  $L$  indicating a much weaker dependence on system size than on string length. The initial and final quenching fields were chosen to be  $h = -2.2$  and  $h = 1.8$  respectively in the ANNNI Hamiltonian with  $J_2 = 1.0$ , such that  $\bar{E}$  lies near the center of the spectrum.

irrespective of integrability or any specific choice of the initial state.

## VIII. THERMALIZATION AND PERSISTENT MEMORY OF FINITE STRINGS

From the generic behavior of the distributions  $Q_n^\pm$  and the post quench domain statistics, it is evident that string observables retain strong memory of the initial ground state even after long times following a chaotic quench. In this section, we attempt to understand this seemingly conflicting behavior of such operators in light of eigenstate thermalization, which on the contrary professes a very fast scrambling of initial state details after chaotic quenches. This strong memory further suggests that the string observables provide a scalable way to recollect initial state information in a system following an ergodic time evolution. Also, the usual validity of ETH in long string-like observables in itself is an important area of current investigations. Therefore, how such observables deviate from a purely microcanonical description after a chaotic quench is what we proceed to address.

The approach of the local string projectors to the complete ground state projector with increasing string length can be seen to manifest in the eigenstate distribution of the diagonal matrix elements  $(P_n)^{\alpha\alpha} = \langle \phi_\alpha | P_n | \phi_\alpha \rangle$ . In Fig. 11(a), we show the distribution of the diagonal matrix elements in the eigenstates of a chaotic ANNNI Hamiltonian. It is observed that as the string length  $n$  increases, the operators quickly become localized near the ground state, reflecting how the probe  $\mathcal{L}_n(t)$  approach the full Loschmidt echo in quenching setups. Further according to ETH, the expectation of local observables following a chaotic quench are expected to be smooth functions

of energy when it is the only conserved quantity in the quench. This implies that the state to state fluctuations between nearby eigenstates,

$$F_\alpha^{(n)} = |(P_n)^{(\alpha+1)(\alpha+1)} - (P_n)^{\alpha\alpha}|, \quad (36)$$

should vanish in the thermodynamic limit along with the nearest neighbor level spacing,

$$|E_{p+1} - E_p| \sim e^{-L}. \quad (37)$$

Therefore, to understand whether the string observables thermalize, we study the distribution  $F_\alpha^{(n)}$  for different string sizes. The mean state to state fluctuation  $\overline{F}^{(n)}$  is obtained by averaging the differences  $F_\alpha^{(n)}$  over high energy eigenstates near the average energy  $\overline{E} = \langle \psi_0 | H | \psi_0 \rangle$ , following a chaotic quench starting from an initial state  $|\psi_0\rangle$ . In Fig. 11(b), we show the dependence of the mean fluctuation on the system size. The mean fluctuation is seen to decay exponentially with system size irrespective of string lengths of the observables. Moreover while the magnitude of fluctuations is strongly suppressed with increasing  $n$ , the slope does not depend on  $n$ . Both observations are consistent with ETH [41, 58, 59] confirming that, as perhaps expected, the string observables satisfy ETH.

We see that the strong memory effects of the initial state in string observables are not coming from any ETH violations. What happens instead is that for string observables their fluctuations rapidly increase with  $n$ . To quantify this effect we consider relative fluctuations of the diagonal matrix elements of  $P_n$  averaged over a narrow energy window:

$$\sigma^{(n)} = \frac{\sqrt{\text{Var}[(P_n)^{\alpha\alpha]}}{|(P_n)^{\alpha\alpha}|}. \quad (38)$$

The averaging is done in a finite energy window  $[\overline{E} - \delta E, \overline{E} + \delta E]$  around the mean energy  $\overline{E}$ . In quenching experiments with a local Hamiltonian, the variance in energy after quench usually scales as  $\sim \sqrt{L}$  with system size. We therefore choose the width of the energy shell to scale as  $\delta E \sim \sqrt{L}$  while calculating fluctuations of the diagonal matrix elements.

We show  $\sigma^{(n)}$  vs. the string size  $n$  for three different system sizes in Fig. 12. We see that these fluctuations rapidly increase with  $n$ . This increase is consistent with the exponential scaling. Moreover these fluctuations only weakly depend on the system size as expected for local observables. Because in a system with local interactions after a global quench energy variance is extensive, large fluctuations of the string operators allow for preserving sharp memory of the initial state. Large fluctuations of observables within a narrow energy window is also closely connected with long lifetimes of these observables as one can construct highly nonequilibrium states within a very

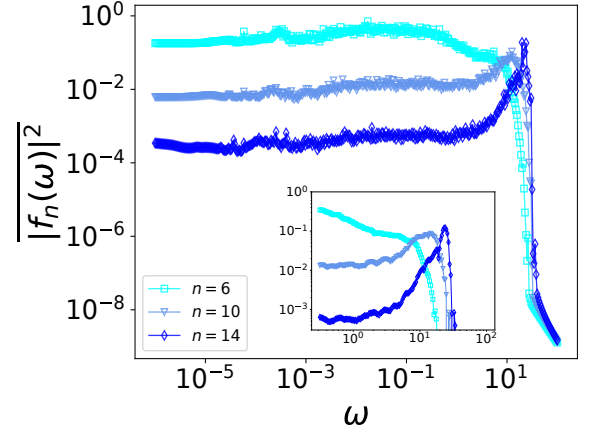


Figure 13. The spectral function of the string observables  $P_n$  averaged over central 50% of the eigenstates in the chaotic ANNNI Hamiltonian with  $J_2 = h = 1$  for  $L = 16$  spins. (Inset) A zoomed-in image of the average spectral function near frequencies where most of the spectral weight is concentrated for longer string operators. With increasing string length, the low frequency spectral function is seen to approach a highly localized distribution indicating late time oscillatory behavior of connected auto-correlation functions (see Eq. (40)).

narrow energy window [60]. To explore this physics for string operators we analyze numerically their spectral function over high energy eigenstates

$$|f_n(E_\alpha, \omega)|^2 = \frac{\sum_{\beta \neq \alpha} |\langle \phi_\alpha | P_n | \phi_\beta \rangle|^2 \delta(\omega_{\alpha\beta} - \omega)}{\langle \phi_\alpha | P_n^2 | \phi_\alpha \rangle_c}, \quad (39)$$

where  $\omega_{\alpha\beta} = E_\alpha - E_\beta$  and  $\delta(\omega) \rightarrow \mu/[2\pi(\omega^2 + \mu^2)]$ , such that  $\mu = 10\omega_{min}$  where  $\omega_{min}$  is the minimum level spacing. To ensure proper normalization of the spectral function, we divide by the eigenstate fluctuations  $\langle P_n^2 \rangle_c = \langle P_n^2 \rangle - \langle P_n \rangle^2$  which is equivalent to the spectral function summed over all frequencies [61].

In Fig. 13 we plot the average spectral function  $\overline{|f_n(\omega)|^2}$  over central 50% of the eigenstates in the nonintegrable ANNNI model. It is seen that for finite strings the average spectral function at low frequencies develop a uniform plateau as predicted by the random matrix limit of ETH. However, with increasing string length, the spectral weight of the string operators quickly approaches a sharply localized monochromatic distribution. Now, it can be shown that the average spectral function is nothing but the Fourier transform of unequal time connected correlation functions of the string operators [39, 62],

$$|f_n(E_\alpha, \omega)|^2 = \frac{1}{4\pi} \int_{-\infty}^{\infty} e^{-i\omega t} \frac{\langle \phi_\alpha | \{P_n(t), P_n(0)\} | \phi_\alpha \rangle_c}{\langle \phi_\alpha | P_n^2 | \phi_\alpha \rangle_c} dt \quad (40)$$

where  $\{\cdot\}$  is the anticommutator and

$$\langle \{P_n(t), P_n(0)\} \rangle_c = \langle \{P_n(t), P_n(0)\} \rangle - 2 \langle P_n(t) \rangle \langle P_n(0) \rangle.$$

Therefore, the spectral function encodes the real-time dynamics of local observables and sets the relaxation

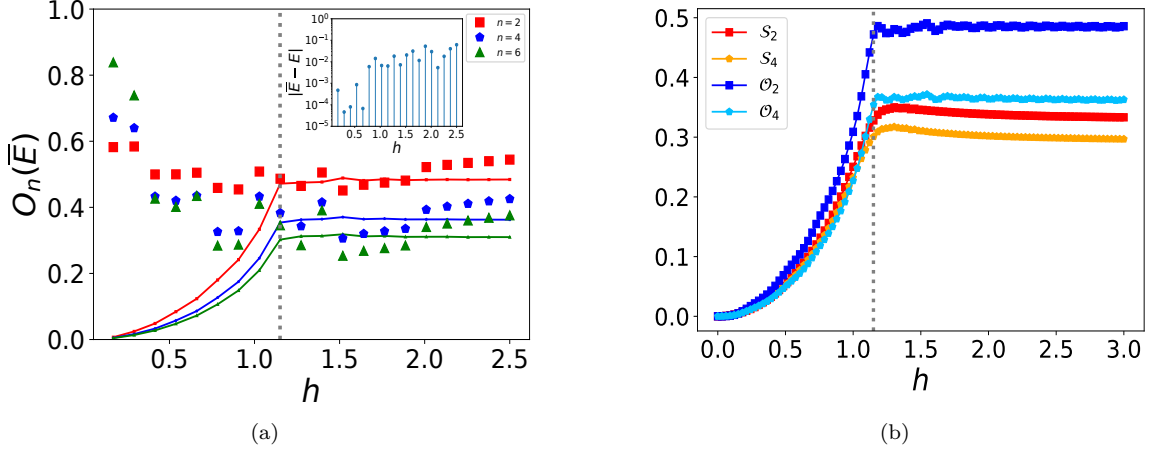


Figure 14. (a) The quantity  $O_n(\bar{E})$  (discrete symbols) against the quenched field  $h$  for different string lengths  $n$ . In contrast to the time averaged projectors  $\mathcal{O}_n$  (solid lines), the single-eigenstate expectations  $O_n(\bar{E})$  fail to detect the equilibrium QCP accurately. (Inset) The difference between the mean energy after quench and energy  $E$  of the actual eigenstate chosen to evaluate  $O_n(\bar{E})$ . This difference is expected to decrease fast with increasing system size. (b) The string probes  $S_n$  contrasted with the local projectors  $\mathcal{O}_n$  for different string lengths  $n$  against the quenched field. Although the probes  $S_n$  develop a maxima near the equilibrium QCP, unlike  $\mathcal{O}_n$  they fail to approach any sharp singularity with increasing string length. In both the panels the quenching simulation has been started from the polarized initial state  $|\rightarrow\rightarrow\dots\rangle$  in a nonintegrable ANNNI model ( $J_2 = 0.1$ ) of  $L = 16$  spins and all time averages have been performed up to  $T = 30$ . The vertical dashed lines indicate the position of the actual QCP in equilibrium.

time scale of  $P_n$  in eigenstates of the chaotic Hamiltonian. The behavior of the spectral function seen in Fig. 13 suggests that the connected correlation functions of long string operators show prominent late-time oscillations in chaotic eigenstates rather than vanishing steadily due to loss of memory (see Appendix. G). This in turn indicates that the string observables indeed have a very long lifetime as compared to single-site observables.

It is now evident that the projectors  $P_n$  have two distinct properties, i.e., (i) with increasing string length they project states onto the completely polarized state  $|\rightarrow\rightarrow\dots\rangle$  and (ii) in quenching experiments, they retain a strong memory of the initial state even after sufficiently long chaotic dynamics. Given this, it is natural to ask which of these features plays a dominant role in capturing the equilibrium QCPs following a quench. To address this question, we study the quantity,

$$O_n(\bar{E}) = -\frac{1}{n} \log \langle \phi_\gamma | P_n | \phi_\gamma \rangle, \quad (41)$$

where  $|\phi_\gamma\rangle$  is an eigenstate of the chaotic ANNNI Hamiltonian  $H$  having energy  $E$  which is closest to the mean energy  $\bar{E}$  after a quench. This quantity  $O_n(\bar{E})$  being closest to the typical value of  $\mathcal{O}_n$  after quench, is not expected to contain any information of the initial state whatsoever. In Fig. 14(a), we contrast the behavior of  $O_n(\bar{E})$  with the time averaged probes  $\mathcal{O}_n$  following different quenches across the equilibrium QCP. However, unlike the time averaged local probes, we do not observe any sharp signature in the quantity  $O_n(\bar{E})$  detecting the equilibrium QCPs.

This suggests that the memory of the initial state in a quench indeed plays an instrumental role in capturing signatures of equilibrium criticality in the string observables.

On the other hand, we construct simpler string operators which do not project onto the polarized state  $|\rightarrow\rightarrow\dots\rangle$ , for example (also see Ref. [26]),

$$S_n = \frac{1}{L} \sum_{i=1}^L \prod_i^{i+n} \sigma_i^x \quad (42)$$

and observe the time insensitive probe

$$\mathcal{S}_n = -\frac{1}{n} \log \lim_{T \rightarrow \infty} \frac{1}{T} \int_0^T dt \langle \psi(t) | S_n | \psi(t) \rangle, \quad (43)$$

following nonintegrable quenches. In Fig. 14(b), we contrast the late time behavior of such observables with that of the local projectors  $\mathcal{O}_n$  after finite but sufficiently long time averaging. The observables  $S_n$  do indeed detect the equilibrium QCPs with a maxima and have an overall similar profile with the quenched field as the probes  $\mathcal{O}_n$ . However, unlike  $\mathcal{O}_n$ , the observables  $S_n$  fail to approach a nonanalyticity and remain smooth with increasing string length. Therefore, one might infer that in addition to the large state-to-state fluctuations, the projecting nature of the strings  $P_n$  allow them to sharply detect equilibrium QCPs while approaching true nonanalyticities associated with the time averaged LE. Whether this connection between the detection of equilibrium QCPs in quenching setups and the memory effect carries forward in a generic sense to arbitrary string observables is an interesting question left for future investigations.

## IX. SUMMARY AND FUTURE DIRECTIONS

In summary, we studied local string observables as probes of quantum phase transitions after quenching a system into highly excited states. We particularly show that one can accurately determine both the position of a quantum critical point and the associated universal critical exponents even long after the system equilibrates into effectively high-temperature states. This analysis applies both to integrable and chaotic systems satisfying the ETH. As we explain in this paper exponentially vanishing with the system size state to state fluctuations of local observables do not prevent the system of retaining memory of the initial state.

We first analyze the long time averaged Loschmidt echo following a generic quench, its rate function develops sharp nonanalyticities, which precisely detect QCPs of the equilibrium system. Along with discontinuous jump singularities in its derivative responses, the nonanalyticities of the time averaged LE can be explained by its topologically different pole structure for quenches across the equilibrium critical point. Further extending the connection of the nonanalyticities with equilibrium criticality, we proceed with a finite size scaling analysis of the time averaged Loschmidt echo and find universal critical exponents associated with the QCPs. The Loschmidt echo can be understood as an expectation value of a particular string operator given by a product of all the spins in the system. Such an operator is very nonlocal and is therefore hard to measure. In order to connect with experimentally relevant observables, we then analyzed finite strings, i.e. operators involving finite products of spins. Interestingly, such string observables develop sharp signatures precisely at equilibrium QCPs of the quenched system even when the string size is very small. In this respect our results are consistent with those recently reported in Ref. [26]. Furthermore, using the local observables we are able to extract critical scaling information and universal exponents associated with equilibrium QCPs even after a long ergodic time evolution.

The local string operators are also found to serve as probability distributions of domain formation in the late time state of a quenched system. We analyzed such distributions revealing an underlying memory of equilibrium critical information encoded in the post quench domain statistics of generic quantum systems. Specifically, the mean longest domain length observed in the late time post quench state, develops a sharp dip precisely near critical points of the equilibrium system. Our results explain recent experiments in trapped ion quantum simulator [17], they also agree with recent numerical works [24, 32] observing sharp signatures in local single-site observables. We explain that emergence of these singularities is due to large fluctuations of string observables.

We also probe the time averaged two-time infinite temperature correlations of the local string observables following a quench. The time averaged auto-correlation and infinite OTOC of the string operators are constructed such that they approach the long time averaged LE as the string size increases. Interestingly, similar sharp features near equilibrium QCPs emerge in the infinite temperature correlators following both integrable and chaotic quenches. These sharp signatures of equilibrium QCPs in infinite temperature correlations also establish the initial state independence of the results.

Finally, given the emergence of critical signatures following a chaotic quench, it seems evident that despite an ergodic evolution, the string observables retain strong memory of the initial ground state. In fact, we show that this persistent memory of the initial state plays a significant role in sharply detecting the equilibrium critical points in quenching experiments. We show that this memory is not a result of ETH violation but are encoded in large state-to-state fluctuations near the mean energy after quench, which increases exponentially with string length. These large fluctuations in the string expectations, prevent a complete thermalization of the observables, thereby preserving initial state information. These increasing state to state fluctuations in a narrow energy shell also hint at longer lifetimes of long string observables in chaotic eigenstates. We verify this using the spectral function of such observables, which essentially encode the structure of their off-diagonal matrix elements in the Hamiltonian spectrum. With increasing string length, the spectral function becomes increasingly localized, signaling late time oscillatory dynamics of their connected auto-correlations. These observations collectively lead to the possibility of a unified approach in which the string observables serve as a scalable probe to systematically access ground state information in generic quenching experiments.

A recent theoretical study [63] has also reported the observation of Kibble-Zurek physics in the early time dynamics of OTOCs (see also Ref. [18]), in quenched one dimensional conformal field theories (CFT). The precise connection between late-time string observables and the Kibble-Zurek scaling of early time OTOCs is yet to be understood. Another intriguing area of study might be to probe the efficacy of the string observables to retain critical information in systems undergoing topological phase transitions. For example, in short-ranged integrable systems, it has been reported [64, 65] that the residual energy following a quench might become nonanalytic at critical points separating topologically inequivalent phases in equilibrium. The exact connection of the residual energy in such systems to the local string observables is yet to be studied.

## ACKNOWLEDGMENTS

We acknowledge the use of QuSpin 0.3.6 for numerical computations. We thank Sourav Bhattacharjee, Diptarka Das and Dries Sels for fruitful discussions. S.B. acknowledges support from a PMRF fellowship, MHRD, India. A.P. acknowledges support from NSF under Grant DMR-2103658, the AFOSR under Grants No. FA9550-16-1-0334 and FA9550-21-1-0342 and SPARC program, MHRD, India. A.D. acknowledges support from SPARC program, MHRD, India and SERB, DST, New Delhi, India.

### Appendix A: Complete pole structure of the time averaged LE

To exactly derive the sharp nonanalyticities of the time averaged quantity  $\mathcal{O}_L$  following critical quenches, we impose periodic boundary conditions on the Hamiltonian Eq. (1) in the integrable limit ( $J_2 = 0$ ). In the thermodynamic limit, one can then rewrite the Hamiltonian in decoupled single-particle momentum sectors as,

$$H = \bigotimes_k H_k, \quad (\text{A1})$$

where,

$$\begin{aligned} H_k &= \vec{h}(k) \cdot \vec{\sigma}, \\ h_x(k) &= -2 \sin k, \\ h_y(k) &= 0, \\ h_z(k) &= -2h - 2 \cos k. \end{aligned} \quad (\text{A2})$$

The eigenstates of the above Hamiltonian at any parameter value can be expressed as Bloch states,

$$\begin{aligned} |+\rangle_k &= \begin{pmatrix} -\cos \theta/2 \\ \sin \theta/2 \end{pmatrix}, \quad |-\rangle_k = \begin{pmatrix} \sin \theta/2 \\ \cos \theta/2 \end{pmatrix}, \\ \text{such that, } \cos \theta &= \frac{h_z(k)}{\sqrt{h_x(k)^2 + h_z(k)^2}}, \end{aligned} \quad (\text{A3})$$

with eigenvalues  $\pm |h(\vec{k})|$  respectively. We start from the ground state of  $H_i(h = h_i)$  and quench the system at time  $t = 0$  to a final set of parameters  $H(h)$  and probe the

logarithmic time averaged LE,  $\mathcal{O}_L$  following the quench. Using the translational invariance of the problem, one arrives at the momentum resolved equivalent of Eq. (5),

$$\mathcal{O}_L = -\frac{1}{\pi} \int_0^\pi dk \log [f_+(k)^2 + f_-(k)^2], \quad (\text{A4})$$

where,

$$\begin{aligned} f_+(k) &= |\langle \psi_k(0) | + \rangle|^2, \\ f_-(k) &= |\langle \psi_k(0) | - \rangle|^2, \end{aligned} \quad (\text{A5})$$

which can be further simplified to,

$$\mathcal{O}_L = -\frac{1}{\pi} \int_0^\pi dk \log \left[ 1 - \frac{1}{2} \sin^2(\theta - \theta_i) \right]. \quad (\text{A6})$$

We solve the integral in Eq. (A6) by an analytic continuation into the complex plane, i.e., we substitute  $z = e^{ik}$ , thereby changing the measure of integration to  $dk = -iz^{-1}dz$ . Using the definition of the Bloch angles in Eq. (A3) we obtain an integration over a closed contour  $C$  which is a unimodular circle about the origin  $z = 0$ ,

$$\mathcal{O}_L = \frac{1}{2\pi i} \oint_C F(z) dz, \quad (\text{A7})$$

where,

$$F = \frac{1}{z} \log \left[ \frac{h^2 (z^2 - 1)^2}{8z(h+z)(hz+1)} + 1 \right]. \quad (\text{A8})$$

We define the measure of a nonanalyticity of  $\mathcal{O}_L$  at the critical point  $h_c = 1$  as,

$$\delta = \left| \partial_{h_c^+} \mathcal{O}_L - \partial_{h_c^-} \mathcal{O}_L \right|, \quad (\text{A9})$$

such that any nonzero  $\delta$  signals a breakdown of continuity of  $\partial_h \mathcal{O}_L$  and hence, analyticity of  $\mathcal{O}_L$ . To analytically probe the jump singularities in the derivative of  $\mathcal{O}_L$  at the equilibrium QCP, we must therefore focus on the first derivative of the function  $F$  with respect to the quenching field  $h$ . The derivative  $\partial_h F$  is found to be a meromorphic function,

$$\partial_h F = \frac{h (z^2 - 1)^2 (hz^2 + h + 2z)}{z(h+z)(hz+1)(h^2z^4 + 6h^2z^2 + h^2 + 8hz^3 + 8hz + 8z^2)}, \quad (\text{A10})$$

with simple poles on the real axis at,

$$\begin{aligned}
z_1 &= -\frac{1}{h}, \quad z_2 = -h, \quad z_3 = 0, \\
z_4 &= \frac{\sqrt{2-h^2} - \sqrt{2}h\sqrt{\frac{3-2\sqrt{2-h^2}}{h^2} - 1} - 2}{h}, \\
z_5 &= \frac{\sqrt{2-h^2} + \sqrt{2}h\sqrt{\frac{3-2\sqrt{2-h^2}}{h^2} - 1} - 2}{h}, \\
z_6 &= \frac{-\sqrt{2-h^2} - \sqrt{2}h\sqrt{\frac{2\sqrt{2-h^2}+3}{h^2} - 1} - 2}{h}, \\
z_7 &= \frac{-\sqrt{2-h^2} + \sqrt{2}h\sqrt{\frac{2\sqrt{2-h^2}+3}{h^2} - 1} - 2}{h}.
\end{aligned} \tag{A11}$$

Fig. 15 shows all the poles of  $\partial_h F$  when the transverse field  $h$  lies in both the paramagnetic and ferromagnetic phase. We note that the pole structure changes abruptly across the quantum critical point  $h = h_c = 1$  resulting in a finite nonzero value of  $\delta$  and consequently a breakdown of analyticity in  $\mathcal{O}_L(h_c)$ . In particular, as seen from Fig. 2 and Fig. 15, the poles represented by  $z_1$  and  $z_2$

exchange their positions with respect to the contour of integration  $C$ , as one moves across the critical point. Similarly, calculating the residues of the relevant poles contributing to the discontinuous jump in the derivative  $\partial_h \mathcal{O}_L$  around the critical point  $h = 1 + \epsilon$  ( $\epsilon \ll 1$ ), we obtain,

$$\begin{aligned}
\text{Residue}(z_1) &= -1 + \epsilon; & \text{Residue}(z_2) &= 1 - \epsilon; \\
& & \text{Residue}(z_3) &= 1 - \epsilon; \\
\text{Residue}(z_5) &= \begin{cases} \sqrt{2}, & \epsilon > 0, \\ -\sqrt{2}, & \epsilon < 0; \end{cases} & \text{Residue}(z_7) &= -\sqrt{2}.
\end{aligned} \tag{A12}$$

To exactly calculate the discontinuous jumps in derivatives, we apply Cauchy's residue theorem,

$$\delta = \left| \sum \text{Residue}(\partial_{h_c^+} F, z_{in}^{para}) - \text{Residue}(\partial_{h_c^-} F, z_{in}^{ferro}) \right|, \tag{A13}$$

where  $z_{in}^{para}$  and  $z_{in}^{ferro}$  are the poles lying inside the contour  $C$  in the paramagnetic and the ferromagnetic phase respectively and the summation is over all the poles. Taking into consideration the residue of the poles in Eq. (A12), we obtain in the limit  $\epsilon \rightarrow 0$ ,

$$\delta = 2(\sqrt{2} - 1) \approx 0.82, \tag{A14}$$

which agrees with the discontinuous jump found numerically in Fig. 1. This explains the development of a jump discontinuity (see Fig. 1) in the derivative of  $\mathcal{O}_L$  at the critical points. When quenched on the critical point, the poles  $z_1$  and  $z_2$  lie exactly on the contour, thus making the observable  $\mathcal{O}_L$  nonanalytic.

## Appendix B: Critical behavior of local projectors in the thermodynamic limit

For shorter strings of length  $n < L$ , the long time averages  $\bar{\mathcal{L}}_n$  can be evaluated exactly by solving the corresponding fermionic problem for integrable quenches in the thermodynamic limit. Through a Jordan-Wigner transformation, the Ising Hamiltonian in Eq. (1) can be rewritten in terms of noninteracting spinless fermions,

$$\begin{aligned}
\sigma_j^z &= 2c_j^\dagger c_j - 1, \\
\sigma_i^x &= (c_i + c_i^\dagger) \prod_{j<i} (1 - 2c_j^\dagger c_j),
\end{aligned} \tag{B1}$$

where the operators  $c_i$  satisfy the standard fermionic algebra. Depending of the fermion parity specified by the operator,

$$\begin{aligned}
P_\pm &= \frac{1}{2} (\mathbb{I} \pm \Sigma), \text{ where,} \\
\Sigma &= \prod_j (2c_j^\dagger c_j - 1) = \prod_j \sigma_j^z,
\end{aligned} \tag{B2}$$

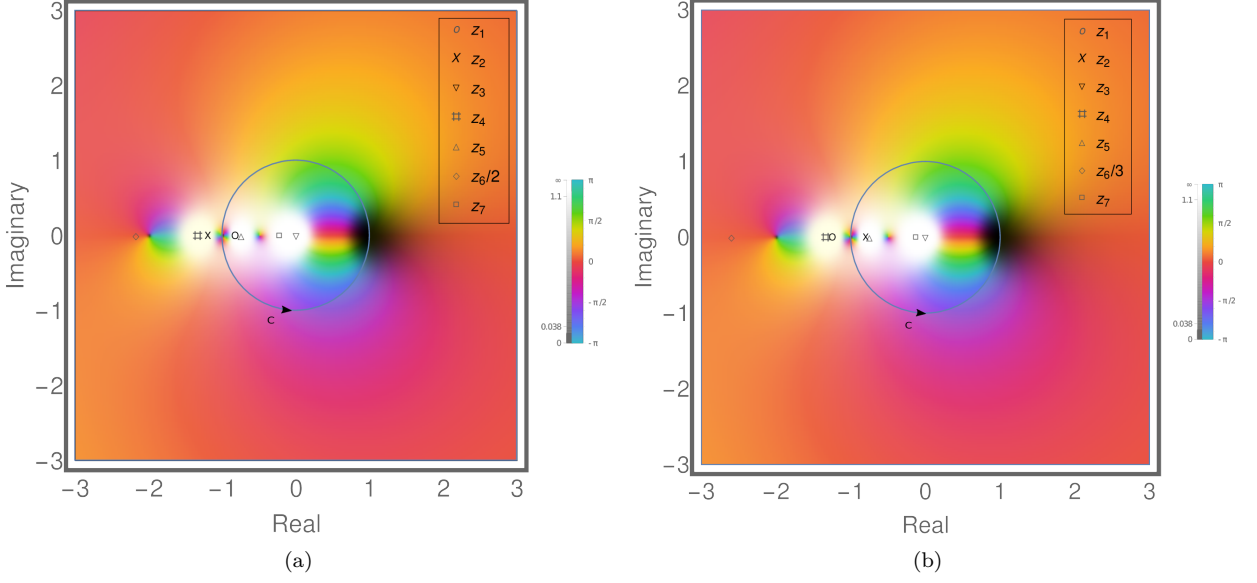


Figure 15. The complete pole structure of the derivative  $\partial_h F$  when analytically continued into the complex plane following a quench to the (a) paramagnetic phase ( $h = 1.2$ ) and the (b) ferromagnetic phase ( $h = 0.8$ ), for  $J_2 = 0$ . The color scheme represents the complex phase whereas white and black colors represent poles and zeros of the function respectively. As is evident from both (a) and (b), the poles  $z_1$  and  $z_2$  exchange their positions with respect to the contour  $C$  as one moves across the critical point. At the critical point the poles are seen to lie on the contour  $C$ , which in turn results in the nonanalyticity of  $\mathcal{O}_L$  at the critical point.

it can be shown that the Hamiltonian can be decoupled into two independent parity sectors,

$$H = P_+ H P_+ + P_- H P_- . \quad (\text{B3})$$

To simplify calculations, we choose the initial state  $|\psi(0)\rangle$  to be the ground state at  $h = 0$  in the even parity sector. Since, the Hamiltonian  $H$  respects parity, the time-evolved state of the system also resides in the same parity sector. Therefore, the expectation value of all strings in  $P_n$  that do not conserve parity vanish identically. It is for this reason that  $P_1$  has a trivial time independent expectation throughout the evolution and we do not consider it in this section. We now express the local projectors in terms of transformed fermionic operators,

$$A_i = c_i^\dagger + c_i \text{ and } B_i = c_i^\dagger - c_i . \quad (\text{B4})$$

In terms of the  $A$  and  $B$  fermions, the short projectors assume the form,

$$P_2 = \frac{1}{2^2 L} \sum_i 1 + B_i A_{i+1},$$

$$P_3 = \frac{1}{2^3 L} \sum_i 1 + 2B_i A_{i+1} + B_i A_{i+1} B_{i+1} A_{i+2} . \quad (\text{B5})$$

Due to the noninteracting nature of the Hamiltonian for  $J_2 = 0$  (see Eq.(1)), while evaluating the late time averages in  $\mathcal{L}_n$ , we use Wick's contraction to decompose longer correlations to algebraic functions of two point correlations. Using this prescription, it can be shown

that in noninteracting systems, for expectation values of strings containing generic fermionic operators  $f_i$  one obtains,

$$\left\langle \prod_{i=1}^l f_i \right\rangle = |\text{Pf}(M)| = \sqrt{\det M}, \quad (\text{B6})$$

where  $M$  is an anti-symmetric  $l \times l$  matrix of two-point correlations such that,

$$M_{\mu\nu} = \langle f_\mu f_\nu \rangle ; 1 < \mu < \nu < l . \quad (\text{B7})$$

We therefore evaluate the two point correlations comprising of the  $A$  and  $B$  fermions in the asymptotic steady state, which will in turn allow us to evaluate the finite projectors. Utilizing the translational invariance of the system and the consequent decoupling into conserved quasi-momenta modes  $k$ , it can be shown that the two point correlators in the steady state assume the form,

$$\langle A_m A_{m+j} \rangle = \langle B_{m+j} B_m \rangle = \delta_{j0},$$

$$\langle A_m B_{m+l} \rangle =$$

$$\frac{1}{2\pi} \int_{-\pi}^{\pi} dk e^{-ilk} e^{-i\theta k} \frac{1 - h \cos k}{\sqrt{1 + h^2 - 2h \cos k}}, \quad (\text{B8})$$

where  $\theta$  is the Bloch angle of the quenched Hamiltonian as also mentioned in Eq. (A3). Also, to simplify calculations, we have repositioned the momentum modes like  $k \rightarrow \pi - k$  with respect to that in Eq. (A2), such that the exact gapless critical mode for the QCP  $h = 1$  now lies at  $k = 0$ . To analytically calculate the expectation of  $P_n$ , we recast

the integrals in Eq. (B8) for quenches near the critical point  $h = 1 + \delta$ ,

$$\langle A_m B_{m-1} \rangle = \frac{1}{\pi} \int_0^\pi C_1(k, \delta) dk, \quad (\text{B9})$$

where,

$$C_1(k, \delta) = \frac{((\delta + 1) \cos(k) - 1)^2}{\delta^2 + 2\delta - 2(\delta + 1) \cos(k) + 2}. \quad (\text{B10})$$

Since, the integrand  $C_1(k, 0)$  has a removable singularity at the point  $k = 0$ , a power series expansion of  $C_1$  about  $\delta = 0$  does not converge everywhere within the interval of integration. In the first approach, to understand the nature of the function  $\mathcal{O}_2$ , we evaluate the integral in Eq. (B9) exactly by an analytic continuation into the

complex plane. Specifically, we substitute  $z = e^{ik}$  to obtain an integration over a closed contour  $C$  which is a unimodular circle about the origin  $z = 0$ ,

$$\langle A_m B_{m-1} \rangle = \frac{1}{2\pi} \oint_C \frac{i(\delta + z(\delta z + z - 2) + 1)^2}{4z^2(-\delta + z - 1)(\delta z + z - 1)} dz. \quad (\text{B11})$$

Note that the integrand in Eq. (B11) is meromorphic with poles at  $z = 0$ ,  $z = 1 + \delta$  and at  $z = (1 + \delta)^{-1}$ . Except the pole at  $z = 0$ , only one of the other two lie inside the contour of integration depending on the sign of  $\delta$ . Therefore, by summing over nonzero residues from the poles, we evaluate the correlations and hence the quantity  $\mathcal{O}_2$ , in the different phases separately as,

$$\mathcal{O}_2 = \begin{cases} -\frac{1}{2} \log \left[ \frac{1}{4} \left\{ 1 + \frac{1}{2} (-\delta^2 - 2\delta + 1) \right\} \right] & \text{for } \delta < 0, \\ -\frac{1}{2} \log \left( \frac{3}{8} \right) & \text{for } \delta > 0. \end{cases} \quad (\text{B12})$$

It is then straight forward to estimate the jump discontinuity in the first derivative of  $\mathcal{O}_2$  exactly at  $\delta = 0$ ,

$$\Delta_2 = |\partial_{\delta^+} \mathcal{O}_2 - \partial_{\delta^-} \mathcal{O}_2| = 0.33. \quad (\text{B13})$$

Similar to the correlation function  $\langle A_m B_{m-1} \rangle$ , we evaluate the correlations contained in  $\mathcal{P}_3$  to obtain,

$$\mathcal{O}_3 = \begin{cases} -\frac{1}{3} \log \left[ \frac{1}{4} (9 - 7\delta(\delta + 2)) \right] & \text{for } \delta < 0, \\ -\frac{1}{3} \log [9/4] & \text{for } \delta > 0. \end{cases} \quad (\text{B14})$$

This gives the discontinuous jump in the first derivative of  $\mathcal{O}_3$  at the critical point  $\delta = 0$  as,

$$\Delta_3 = |\partial_{\delta^+} \mathcal{O}_3 - \partial_{\delta^-} \mathcal{O}_3| = 0.51. \quad (\text{B15})$$

By performing higher order Wick's contractions (see Eq. (B6)), it is then possible to exactly calculate the late time expectation of  $\mathcal{P}_n$  for arbitrary string lengths.

Another approach to probe the critical nature of the observables  $\mathcal{O}_n$  is to regularize the integrals like in Eq. (B9) near the critical point. To numerically evaluate the integrals, we introduce an infrared cutoff  $\epsilon$ ,

$$\langle A_m B_{m-1} \rangle \rightarrow \frac{1}{\pi} \int_\epsilon^\pi C_1(k, \delta) dk, \quad (\text{B16})$$

such that  $\epsilon \ll |\delta|$  and  $\epsilon \ll n^{-1}$ . The condition  $\epsilon \ll |\delta|$  ensures that the length  $\epsilon^{-1}$  is much larger than the correlation length  $\delta^{-1}$  near the critical point. In passing we note that a cutoff scale  $\epsilon$  near the exact critical point naturally arises when dealing with finite size systems as  $\epsilon \sim L^{-1}$ . The condition  $\epsilon \ll n^{-1}$  in such a situation ensures that we are in a regime where the observables scale with the shorter length  $n$  rather than with  $\epsilon^{-1} \sim L$ . Following this regularization, the function  $C_1(k, \delta)$  becomes well behaved everywhere within the interval of integration  $[\epsilon, \pi]$ . To understand how the derivatives diverge in lowest order, we then expand the function  $C_1(k, \delta)$  as a power series near  $\delta = 0$  up to quadratic order and perform the integral in Eq. (B16) to finally obtain,

$$\mathcal{O}_2 \approx -\frac{1}{2} \log \left[ \frac{1}{8} \left\{ \delta^2 \left( \frac{\epsilon - \pi}{2} + \cot \left( \frac{\epsilon}{2} \right) \right) + \frac{\delta(\epsilon + \sin(\epsilon) - \pi)}{\pi} + 3 \right\} \right]. \quad (\text{B17})$$

In Fig. 3(b) and Fig. 16(a), we numerically show the discontinuous jumps of the first derivative and divergences in the second derivative of  $\mathcal{O}_2$ ,  $\mathcal{O}_3$  and  $\mathcal{O}_4$  near the crit-

ical point with a lower cutoff  $\epsilon = 0.01$ . The rescaled derivatives  $n^{-1} \partial_\delta^2 \mathcal{O}_n$  when plotted against  $n\delta$ , collapse near the critical point for different  $n$ , where  $0 < \epsilon \ll |\delta|$ .

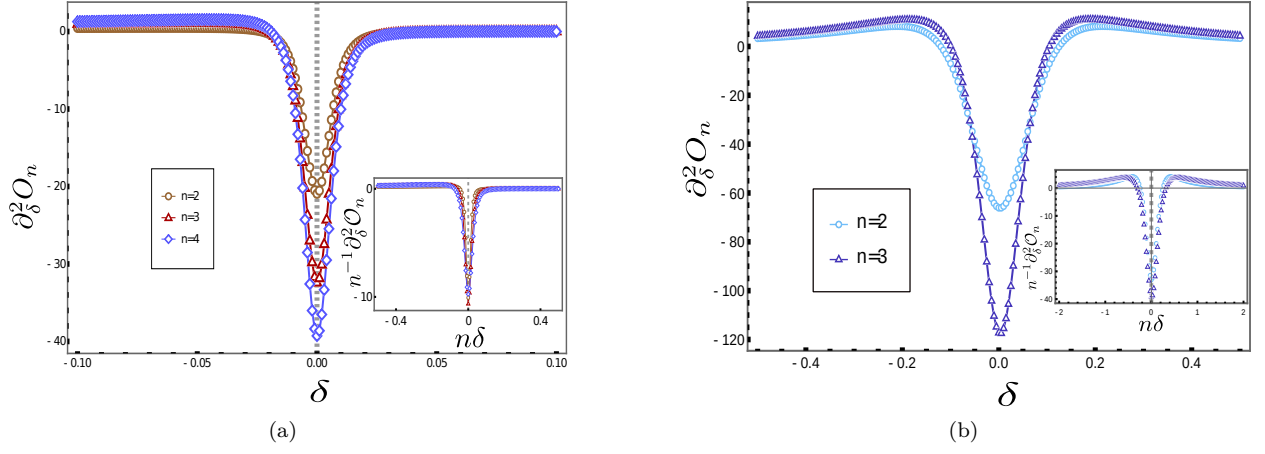


Figure 16. (a) The divergence of the second derivative of the finite observables  $\mathcal{O}_2, \mathcal{O}_3$  and  $\mathcal{O}_4$  calculated numerically, in a thermodynamically large integrable Ising chain near the critical point  $\delta = 0$ , following a quench starting from the initial ground state at  $h_i = 0, J_2 = 0$  to  $h_f = 1 + \delta, J_2 = 0$ . The cutoff scale  $\epsilon$  has been chosen to be 0.01 (see Eq. (B16) and the discussion following it). (Inset) The rescaled derivatives  $n^{-1} \partial_\delta^2 \mathcal{O}_n$  collapse into a single curve for  $\epsilon \ll |\delta|$  near the critical point. (b) The bare and (Inset) rescaled derivatives  $n^{-1} \partial_\delta^2 \mathcal{O}_n$  of the probes  $\mathcal{O}_2$  and  $\mathcal{O}_3$  constructed from the series expansions truncated up to quadratic order, such as in Eq. (B17) with  $\epsilon = 0.01$ .

The exact jump discontinuities in the first derivatives  $\Delta_2$  and  $\Delta_3$  found in this appendix (Eq. (B13) and Eq. (B15) respectively) agree very well with the jump discontinuities shown in Fig. 3(b). Also, exactly at the critical point  $\delta = 0$ , the second derivatives diverge as,

$$\partial_\delta^2 \mathcal{O}_2 |_{\delta=0} \sim -\frac{2}{3\epsilon}, \quad (\text{B18})$$

$$\partial_\delta^2 \mathcal{O}_3 |_{\delta=0} \sim -\frac{32}{27\epsilon}, \quad (\text{B19})$$

when the correlators are evaluated up to a quadratic order in  $\delta$  near  $\delta = 0$ , thus reflecting the discontinuity of the first derivatives at the critical point in the thermodynamic limit.

### Appendix C: Emergence of finite-size scaling

In Appendix. A, we discussed how in the thermodynamic limit, the time averaged Loschmidt echo  $\mathcal{O}_L$  follow-

ing a sudden integrable quench reduces to the expression,

$$\mathcal{O}_L = -\frac{1}{\pi} \int_0^\pi dk \log \left[ 1 - \frac{1}{2} \sin^2(\theta - \theta_i) \right], \quad (\text{C1})$$

where,

$$\cos \theta = \frac{h_z(k)}{\sqrt{h_x(k)^2 + h_z(k)^2}}, \quad (\text{C2})$$

$\theta_i$  and  $\theta$  being the Bloch angles representing the single particle Hamiltonian  $H_k = \vec{h}(k) \cdot \vec{\sigma}$  (see Eq. (A2)), before and after the quench, respectively. At the critical point ( $h = h_c$ ), the Bloch angle  $\theta$  is not well-defined. Rather, the angles  $\theta_{k=\pi,0}(h = \pm 1)$  assume indeterminate 0/0 forms in the thermodynamic limit. Therefore, the integrand Eq. (C1) is ill defined at the isolated critical points.

However, as argued in Sec. V, the observable  $\mathcal{O}_L$  for finite systems, exhibit universal critical scaling near the equilibrium critical point. To see the emergence of the scaling theory, we proceed to analytically evaluate the integral in Eq. (C1) following quenches in finite size systems. As also seen in Sec. III, the critical singularity drifts towards the momentum  $k_c = \pi$  as one approaches the critical point  $h_c = 1$ . Expanding the integral in Eq. (C1) near the critical point we obtain,

$$\mathcal{O}_L \approx -\frac{1}{\pi} \int_0^\pi dk \log \left[ 1 - \frac{1}{2} \sin^2 \left( \frac{k}{2} \right) - \frac{\delta}{2} \sin^2 \left( \frac{k}{2} \right) + \frac{1}{8} \delta^2 \tan^2 \left( \frac{k}{2} \right) \right], \quad (\text{C3})$$

where  $h = 1 + \delta$ . From Eq. (C3) it is evident that exactly

at the mode  $k = \pi$ , the term quadratic in  $\delta$  in  $\mathcal{O}_L$

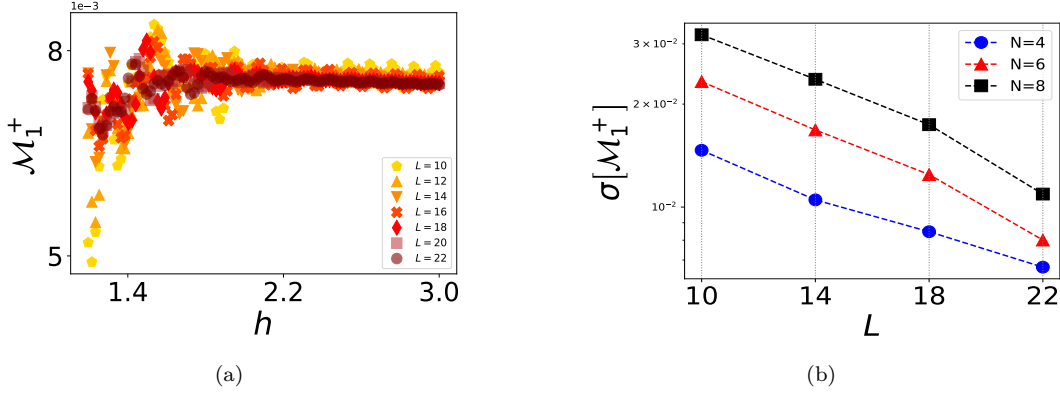


Figure 17. (a) The distribution  $\mathcal{M}_1^+$  after  $N = 10$  uncorrelated measurements against the quenched field  $h$ , for quenches into the paramagnetic phase in a chaotic ANNNI model. The distribution is seen to approach a slowly varying function of the quenched field  $h$  with increasing system size  $L$  (a darker color represents a higher system size). (b) The relative deviation of  $\mathcal{M}_1^+$  from its mean decreases rapidly with increasing system size irrespective of the number of measurements  $N$ . In both the panels the quench was started from a completely polarized initial state  $|\rightarrow \rightarrow \dots\rangle$ .

diverges. This divergence in the second derivative reflects the emerging nonanalyticity of  $\mathcal{O}_L$  near the equilibrium QCP. We therefore estimate the singular part of  $\mathcal{O}_L$  by focusing on the contribution to the integral from the critical mode  $k = \pi$ .

However, since we are dealing with systems having a finite size  $L$ , the integral in Eq. (C3) has to be approximated by a finite Riemann sum in discrete momenta separated by  $dk \sim \pi/L$ . With increasing system size,  $k$  assumes continuous values and modes near the critical mode  $k = \pi - \epsilon$ , approach  $k = \pi$  as  $\epsilon \sim L^{-1}$ . Therefore, to study the singular part of the integral in Eq. (C3), we expand it near  $k_c$  by substituting  $k = k_c - \epsilon$ . Further using  $\epsilon \sim L^{-1}$ , we obtain in leading order for the singular part,

$$\mathcal{O}_L^c \approx -\frac{1}{L} \log \left[ \frac{1}{2} + \frac{x^2}{2} + \mathcal{O}\left(\frac{x}{L}\right) \right], \quad (\text{C4})$$

where  $x = \delta L$  is dimensionless. For  $x = \delta L \ll 1$ ,  $L$  being the smallest length, we expect the emergence of finite size critical scaling in the singular part  $\mathcal{O}_L^c$  with system size  $L$ . In this scaling regime we can hence approximate,

$$\mathcal{O}_L^c \approx -\frac{1}{L} \left( x^2 + \frac{x^4}{2} + \mathcal{O}(x^6) \right), \quad (\text{C5})$$

such that,

$$\mathcal{O}_L^c \approx L^{-1} \Phi(\delta L), \quad (\text{C6})$$

where  $\Phi$  is a scale invariant universal scaling function. This validates our scaling ansatz in Eq. (13) for  $\nu = \alpha = 1$ . Also, from Eq. (C4) it is clear that for sufficiently large but finite system sizes, the singular part approaches zero as the QCP is approached with  $\delta$ . Thus, exactly at the critical point in finite systems,  $\mathcal{O}_L$  can be estimated by the analytic nonsingular part of the integral in Eq. (C1).

Hence, to extract the critical scaling in the singular part of the time averaged Loschmidt echo in Sec. IV, we show a scaling collapse of  $L|\mathcal{O}_L(h_c + \delta) - \mathcal{O}_L(h_c)|$  against  $\delta L$  near the QCP.

#### Appendix D: Suppression of noise with increasing system size

In Sec. VI, we noted that the late-time domain distributions in the paramagnetic phase changes very slowly with the quenched field  $h$ , apart from small fluctuations (see Eq. (21) and Fig. 8). We argue that this noise in the numerical data, particularly for quenches into the disordered phase, is due to a finite system size. In this regard, Fig. 17(a) shows that for quenches into the paramagnetic phase, the long time averaged distribution  $\mathcal{M}_1^+$  after  $N = 10$  uncorrelated measurements, gradually approaches a slowly varying function of  $h$  with increasing system sizes. Furthermore, the relative deviation of  $\mathcal{M}_1^+$  from its mean over different quenched fields in the disordered phase,

$$\sigma[\mathcal{M}_1^+] = \frac{\sqrt{\text{Var}[\mathcal{M}_1^+]}}{\mathcal{M}_1^+}, \quad (\text{D1})$$

decreases fast with increasing system size (see Fig. 17(b)) irrespective of the number of measurements  $N$ . Thus, in the thermodynamic limit, the functions  $\mathcal{M}_n^+$  indeed approach a smooth distribution with the quenched field in the paramagnetic phase. This is also shown for an integrable quench in the thermodynamic limit in Fig. 3(a).

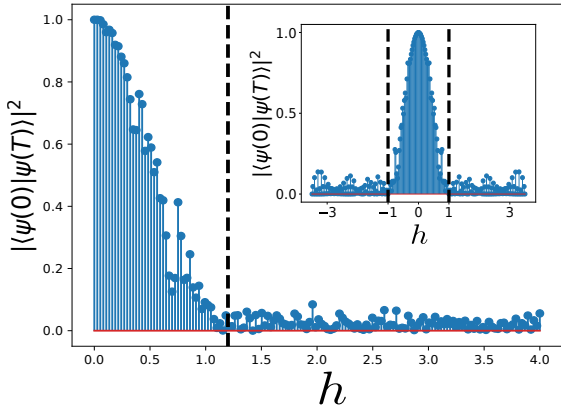


Figure 18. Overlap of the polarized initial state with the late time state following a quench in the nonintegrable ANNNI model ( $J_2 = 0.1$ ) starting from a completely polarized state  $|\rightarrow \rightarrow \dots\rangle$  to a transverse field  $h$  in a system consisting of  $L = 20$  spins for  $T = 30$ . (Inset) The corresponding distribution following an integrable quench. The vertical dashed lines indicate the analytical position of the critical point in both the plots.

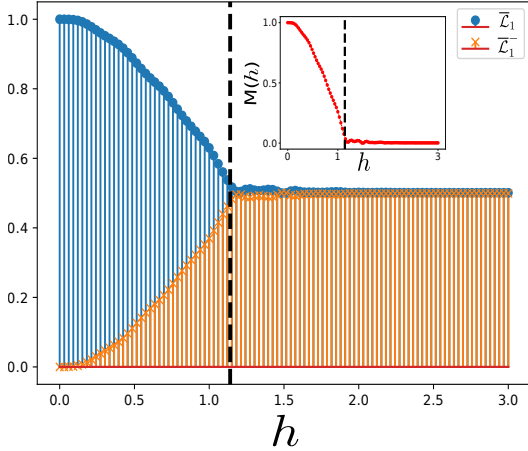


Figure 19. Time averaged expectation of polarized single-spin projectors with respect to the quenched transverse field  $h$ , averaged up to  $T = 30$  following a quench in the chaotic ANNNI model ( $J_2 = 0.1$ ). (Inset) The time averaged longitudinal magnetization density vanishes following quenches into the disordered phase. The time evolution was started from a polarized unentangled initial  $|\rightarrow \rightarrow \dots\rangle$ , in a system consisting of  $L = 18$  spins.

### Appendix E: Overlap of a polarized initial state with the post-quench state

In Sec. VI, we observed that it is more likely to observe a completely polarized string in the late time state following quenches starting from a polarized state into the ordered phase. In Fig. 18, we demonstrate this explicitly by plotting the overlap between the complete initial and time evolved states  $\lim_{t \rightarrow \infty} |\langle \psi(0) | \psi(t) \rangle|^2$  with respect to the quenched transverse field following both nonintegrable and integrable quenches. As seen in Fig. 18, the

completely polarized initial state has a significant overlap with the late time post-quench state for quenches in the ferromagnetic phase but the overlap becomes negligibly small following quenches into the paramagnetic phase.

### Appendix F: Time averaged local magnetization

As argued in Sec. VI, unlike quenches into the ordered phase, following quenches into the paramagnetic phase, domains of both polarizations contribute equally in the long time state. This can be explicitly seen by observing the behavior of long time averaged local magnetization following chaotic quenches (see also Ref. [24, 32]). In Fig. 19, we see that the time averaged expectation of single-spin projectors  $\bar{\mathcal{L}}_1$  ( $\bar{\mathcal{L}}_1^-$ ) into local  $\rightarrow$  ( $\leftarrow$ )-spin polarizations, collapse into a single curve following quenches into the paramagnetic phase. This directly leads to the vanishing of local magnetization density,

$$M(h) = \bar{\mathcal{L}}_1 - \bar{\mathcal{L}}_1^-, \quad (\text{F1})$$

after sufficiently long times following a chaotic quench.

### Appendix G: Off-diagonal matrix elements and relaxation dynamics of string operators

Fig. 20 shows the behavior of the offdiagonal matrix elements of string observables  $P_n$  in the basis of a chaotic ANNNI Hamiltonian  $H$  with increasing string length  $n$ . It is seen that the long string observables generally have a nonuniform distribution of small matrix elements near the middle of the spectrum while connecting states differing by comparatively higher energies. Furthermore, in Sec. VIII we observed that the low frequency spectral function of string operators approaches a sharply peaked distribution with increasing string length. This suggests late time oscillations in their real-time connected correlation functions about zero (see Eq. (40)), in an eigenstate  $|\phi_\alpha\rangle$

$$C_n^\alpha(t) = \frac{1}{2} \frac{\langle \phi_\alpha | \{P_n(t), P_n(0)\} | \phi_\alpha \rangle_c}{\langle \phi_\alpha | P_n^2 | \phi_\alpha \rangle_c}. \quad (\text{G1})$$

In Fig. 21 we see that this is indeed what happens. Particularly, we plot the average connected correlation function  $C_n(t)$  over a few central eigenstates of the chaotic Hamiltonian. To further quantify the late time oscillations in the connected correlations, we calculate the variance,

$$\Delta C_n = \frac{\sqrt{\overline{C_n^2} - \overline{C_n}^2}}{\overline{C_n}}, \quad (\text{G2})$$

where the bar  $\overline{(\cdot)}$  represents time averaging. While the variance is ideally expected to be  $O(1)$  for local observables, we find that for long string operators, the fluctuations increase exponentially with string length.

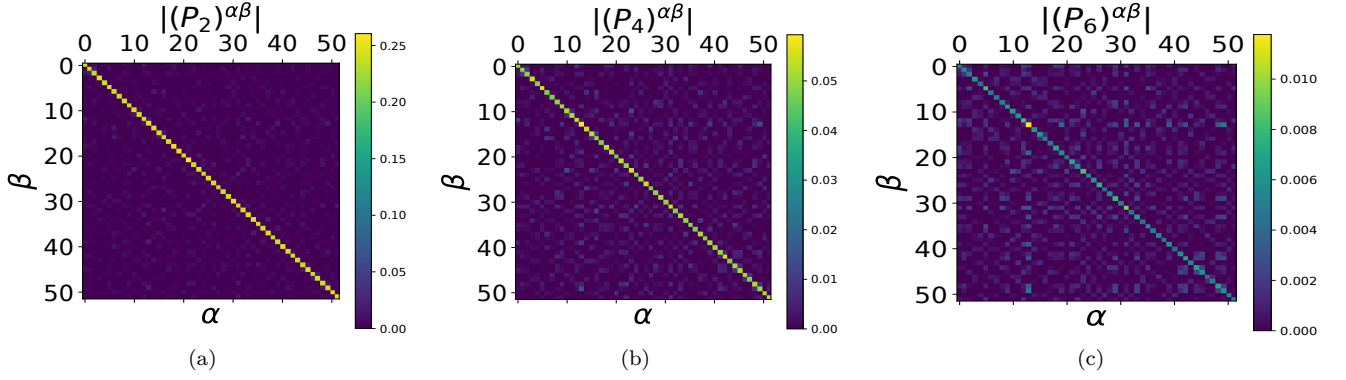


Figure 20. The matrix elements of the string operators  $P_n$  in 50 eigenstates about the center of the spectrum of a chaotic ANNNI Hamiltonian ( $J_2 = 1$ ,  $h = 1$ ) for string lengths (a)  $n = 2$ , (b)  $n = 4$  and (c)  $n = 6$ . The matrix elements have been calculated only in the momentum  $k = 0$  sector of the Hamiltonian for  $L = 16$  spins.

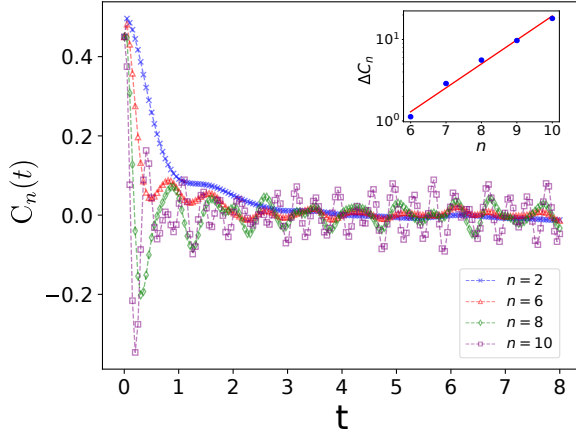


Figure 21. The connected auto-correlation function against time  $t$  of string observables averaged over 20 eigenstates about the center of the spectrum of the chaotic ANNNI Hamiltonian  $H$  with  $J_2 = h = 1$  for  $L = 14$  spins. After long times, longer string operators show faster oscillations with increasing amplitudes, indicating that they have comparatively longer lifetimes as compared to single-site observables. (Inset) The time averaged fluctuations for long string observables increases exponentially with string length.

- 
- [1] P. M. Chaikin and T. C. Lubensky, *Principles of Condensed Matter Physics* (Cambridge University Press, 1995).
- [2] N. Goldenfeld, *Lectures on Phase Transitions and the Renormalization Group (1st ed.)* (CRC Press, 1992).
- [3] H. E. Stanley, Introduction to phase transitions and critical phenomena, *American Journal of Physics* **40**, 927 (1972), <https://doi.org/10.1119/1.1986710>.
- [4] S. Sachdev, *Quantum Phase Transitions*, 2nd ed. (Cambridge University Press, 2011).
- [5] A. Dutta, G. Aeppli, B. K. Chakrabarti, U. Divakaran, T. F. Rosenbaum, and D. Sen, *Quantum Phase Transitions in Transverse Field Spin Models: From Statistical Physics to Quantum Information* (Cambridge University Press, 2015).
- [6] D. Rossini and E. Vicari, Coherent and dissipative dynamics at quantum phase transitions, *Physics Reports* **936**, 1 (2021).
- [7] A. Polkovnikov, K. Sengupta, A. Silva, and M. Vengalattore, Colloquium: Nonequilibrium dynamics of closed interacting quantum systems, *Rev. Mod. Phys.* **83**, 863 (2011).
- [8] M. Heyl, A. Polkovnikov, and S. Kehrein, Dynamical quantum phase transitions in the transverse-field ising

- model, *Phys. Rev. Lett.* **110**, 135704 (2013).
- [9] C. Karrasch and D. Schuricht, Dynamical phase transitions after quenches in nonintegrable models, *Phys. Rev. B* **87**, 195104 (2013).
- [10] J. N. Kriel, C. Karrasch, and S. Kehrein, Dynamical quantum phase transitions in the axial next-nearest-neighbor ising chain, *Phys. Rev. B* **90**, 125106 (2014).
- [11] S. Sharma, U. Divakaran, A. Polkovnikov, and A. Dutta, Slow quenches in a quantum ising chain: Dynamical phase transitions and topology, *Phys. Rev. B* **93**, 144306 (2016).
- [12] M. Heyl, Dynamical quantum phase transitions: a review, *Reports on Progress in Physics* **81**, 054001 (2018).
- [13] S. Bhattacharjee and A. Dutta, Dynamical quantum phase transitions in extended transverse ising models, *Phys. Rev. B* **97**, 134306 (2018).
- [14] P. Jurcevic, H. Shen, P. Hauke, C. Maier, T. Brydges, C. Hempel, B. P. Lanyon, M. Heyl, R. Blatt, and C. F. Roos, Direct observation of dynamical quantum phase transitions in an interacting many-body system, *Phys. Rev. Lett.* **119**, 080501 (2017).
- [15] S. Peotta, F. Brange, A. Deger, T. Ojanen, and C. Flindt, Determination of dynamical quantum phase transitions in strongly correlated many-body systems using loschmidt cumulants, *Phys. Rev. X* **11**, 041018 (2021).
- [16] P. Zanardi, H. T. Quan, X. Wang, and C. P. Sun, Mixed-state fidelity and quantum criticality at finite temperature, *Phys. Rev. A* **75**, 032109 (2007).
- [17] J. Zhang, G. Pagano, P. Hess, A. Kyprianidis, P. Becker, H. Kaplan, A. Gorshkov, Z.-X. Gong, and C. Monroe, Observation of a many-body dynamical phase transition with a 53-qubit quantum simulator, *Nature* **551**, 601 (2017).
- [18] M. Heyl, F. Pollmann, and B. Dóra, Detecting equilibrium and dynamical quantum phase transitions in ising chains via out-of-time-ordered correlators, *Phys. Rev. Lett.* **121**, 016801 (2018).
- [19] A. Keesling, A. Omran, H. Levine, H. Bernien, H. Pichler, S. Choi, R. Samajdar, S. Schwartz, P. Silvi, S. Sachdev, P. Zoller, M. Endres, M. Greiner, V. Vuletic, and M. D. Lukin, Quantum kibble-zurek mechanism and critical dynamics on a programmable rydberg simulator, *Nature* **568**, 207 (2019).
- [20] C. B. Dag, K. Sun, and L. Duan, Detection of quantum phases via out-of-time-order correlators, *Phys. Rev. Lett.* **123**, 140602 (2019).
- [21] P. Titum, J. T. Iosue, J. R. Garrison, A. V. Gorshkov, and Z.-X. Gong, Probing ground-state phase transitions through quench dynamics, *Phys. Rev. Lett.* **123**, 115701 (2019).
- [22] P. Titum and M. F. Maghrebi, Nonequilibrium criticality in quench dynamics of long-range spin models, *Phys. Rev. Lett.* **125**, 040602 (2020).
- [23] K. L. Zhang and Z. Song, Quantum phase transition in a quantum ising chain at nonzero temperatures, *Phys. Rev. Lett.* **126**, 116401 (2021).
- [24] C. B. Dag, P. Uhrich, and J. C. Halimeh, Probing equilibrium and dynamical criticality through single-site observables (2021), [arXiv:2105.05986 \[cond-mat.quant-gas\]](https://arxiv.org/abs/2105.05986).
- [25] C. B. Dag, P. Uhrich, I. P. McCulloch, and J. C. Halimeh, Detecting quantum phase transitions in nonintegrable and long-range ising chains using spatially minimal measurements (2021), [arXiv:2110.02995 \[cond-mat.quant-gas\]](https://arxiv.org/abs/2110.02995).
- [26] A. Haldar, K. Mallayya, M. Heyl, F. Pollmann, M. Rigol, and A. Das, Signatures of quantum phase transitions after quenches in quantum chaotic one-dimensional systems, *Phys. Rev. X* **11**, 031062 (2021).
- [27] L. Villa, S. J. Thomson, and L. Sanchez-Palencia, Finding the phase diagram of strongly correlated disordered bosons using quantum quenches, *Phys. Rev. A* **104**, 023323 (2021).
- [28] K. Chinni, P. M. Poggi, and I. H. Deutsch, Effect of chaos on the simulation of quantum critical phenomena in analog quantum simulators, *Phys. Rev. Research* **3**, 033145 (2021).
- [29] K.-B. Huh, K. Ikeda, V. Jahnke, and K.-Y. Kim, Diagnosing first- and second-order phase transitions with probes of quantum chaos, *Phys. Rev. E* **104**, 024136 (2021).
- [30] S. Paul, P. Titum, and M. F. Maghrebi, Hidden quantum criticality and entanglement in quench dynamics (2022), [arXiv:2202.04654 \[cond-mat.quant-gas\]](https://arxiv.org/abs/2202.04654).
- [31] S. Kheiri, H. Cheraghi, and S. Mahdavifar, Amplifying quantum correlations with quench dynamics in a quantum spin chain: Steady-states versus ground-states (2022), [arXiv:2202.06341 \[quant-ph\]](https://arxiv.org/abs/2202.06341).
- [32] D. Rossini and E. Vicari, Dynamics after quenches in one-dimensional quantum ising-like systems, *Phys. Rev. B* **102**, 054444 (2020).
- [33] M. Schmitt and S. Kehrein, Dynamical quantum phase transitions in the kitaev honeycomb model, *Phys. Rev. B* **92**, 075114 (2015).
- [34] B. Zhou, C. Yang, and S. Chen, Signature of a nonequilibrium quantum phase transition in the long-time average of the loschmidt echo, *Phys. Rev. B* **100**, 184313 (2019).
- [35] J. C. Halimeh, D. Trapin, M. Van Damme, and M. Heyl, Local measures of dynamical quantum phase transitions, *Phys. Rev. B* **104**, 075130 (2021).
- [36] S. Bandyopadhyay, A. Polkovnikov, and A. Dutta, Observing dynamical quantum phase transitions through quasilocal string operators, *Phys. Rev. Lett.* **126**, 200602 (2021).
- [37] M. Rigol, V. Dunjko, V. Yurovsky, and M. Olshanii, Relaxation in a completely integrable many-body quantum system: An ab initio study of the dynamics of the highly excited states of 1d lattice hard-core bosons, *Phys. Rev. Lett.* **98**, 050405 (2007).
- [38] S. Nandy, A. Sen, A. Das, and A. Dhar, Eigenstate gibbs ensemble in integrable quantum systems, *Phys. Rev. B* **94**, 245131 (2016).
- [39] M. Srednicki, The approach to thermal equilibrium in quantized chaotic systems, *Journal of Physics A: Mathematical and General* **32**, 1163 (1999).
- [40] M. Rigol, V. Dunjko, and M. Olshanii, Thermalization and its mechanism for generic isolated quantum systems, *Nature* **452**, 854 (2008).
- [41] L. D'Alessio, Y. Kafri, A. Polkovnikov, and M. Rigol, From quantum chaos and eigenstate thermalization to statistical mechanics and thermodynamics, *Advances in Physics* **65**, 239 (2016), <https://doi.org/10.1080/00018732.2016.1198134>.
- [42] A. Russomanno, M. Fava, and M. Heyl, Quantum chaos and ensemble inequivalence of quantum long-range ising chains, *Phys. Rev. B* **104**, 094309 (2021).
- [43] V. Alba and P. Calabrese, Quantum information scrambling after a quantum quench, *Phys. Rev. B* **100**, 115150 (2019).
- [44] D. Leibfried, R. Blatt, C. Monroe, and D. Wineland, Quantum dynamics of single trapped ions, *Rev. Mod. Phys.* **75**, 281 (2003).

- [45] S. Maldacena Juan, S. H., and S. Douglas, A bound on chaos, *Journal of High Energy Physics* **2016**, 106 (2016).
- [46] S. Xu and B. Swingle, Locality, quantum fluctuations, and scrambling, *Phys. Rev. X* **9**, 031048 (2019).
- [47] B. Yan, L. Cincio, and W. H. Zurek, Information scrambling and loschmidt echo, *Phys. Rev. Lett.* **124**, 160603 (2020).
- [48] B. Swingle, G. Bentsen, M. Schleier-Smith, and P. Hayden, Measuring the scrambling of quantum information, *Phys. Rev. A* **94**, 040302 (2016).
- [49] S. Pappalardi, A. Polkovnikov, and A. Silva, Quantum echo dynamics in the Sherrington-Kirkpatrick model, *SciPost Phys.* **9**, 21 (2020).
- [50] B. V. Fine, T. A. Elsayed, C. M. Kropf, and A. S. de Wijn, Absence of exponential sensitivity to small perturbations in nonintegrable systems of spins 1/2, *Phys. Rev. E* **89**, 012923 (2014).
- [51] T. A. Elsayed and B. V. Fine, Sensitivity to small perturbations in systems of large quantum spins, *Physica Scripta* **T165**, 014011 (2015).
- [52] R. J. Lewis-Swan, A. Safavi-Naini, J. J. Bollinger, and A. M. Rey, Unifying scrambling, thermalization and entanglement through measurement of fidelity out-of-time-order correlators in the dicke model, *Nature Communications* **10**, 1581 (2019).
- [53] J. Zeiher, J.-y. Choi, A. Rubio-Abadal, T. Pohl, R. van Bijnen, I. Bloch, and C. Gross, Coherent many-body spin dynamics in a long-range interacting ising chain, *Phys. Rev. X* **7**, 041063 (2017).
- [54] M. Beccaria, M. Campostrini, and A. Feo, Density-matrix renormalization-group study of the disorder line in the quantum axial next-nearest-neighbor ising model, *Phys. Rev. B* **73**, 052402 (2006).
- [55] P. Weinberg and M. Bukov, QuSpin: a Python Package for Dynamics and Exact Diagonalisation of Quantum Many Body Systems part I: spin chains, *SciPost Phys.* **2**, 003 (2017).
- [56] P. Weinberg and M. Bukov, QuSpin: a Python Package for Dynamics and Exact Diagonalisation of Quantum Many Body Systems. Part II: bosons, fermions and higher spins, *SciPost Phys.* **7**, 20 (2019).
- [57] D. Trapin, J. C. Halimeh, and M. Heyl, Unconventional critical exponents at dynamical quantum phase transitions in a random ising chain, *Phys. Rev. B* **104**, 115159 (2021).
- [58] H. Kim, T. N. Ikeda, and D. A. Huse, Testing whether all eigenstates obey the eigenstate thermalization hypothesis, *Phys. Rev. E* **90**, 052105 (2014).
- [59] J. R. Garrison and T. Grover, Does a single eigenstate encode the full hamiltonian?, *Phys. Rev. X* **8**, 021026 (2018).
- [60] A. Dymarsky, Mechanism of macroscopic equilibration of isolated quantum systems, *Phys. Rev. B* **99**, 224302 (2019).
- [61] D. Sels and A. Polkovnikov, Dynamical obstruction to localization in a disordered spin chain, *Phys. Rev. E* **104**, 054105 (2021).
- [62] C. Schönle, D. Jansen, F. Heidrich-Meisner, and L. Vidmar, Eigenstate thermalization hypothesis through the lens of autocorrelation functions, *Phys. Rev. B* **103**, 235137 (2021).
- [63] A. S. Aramthottil, D. Das, S. Das, and B. Dey, Scrambling under quench (2021), [arXiv:2109.02132 \[hep-th\]](https://arxiv.org/abs/2109.02132).
- [64] S. Bhattacharyya, S. Dasgupta, and A. Das, Signature of a continuous quantum phase transition in non-equilibrium energy absorption: Footprints of criticality on higher excited states, *Scientific Reports* **5**, 16490 (2015).
- [65] S. Roy, R. Moessner, and A. Das, Locating topological phase transitions using nonequilibrium signatures in local bulk observables, *Phys. Rev. B* **95**, 041105 (2017).